ESD-TDR-65-493

Technical Report

384

Magnetic Studies of the Antiferromagnet $RbMnF_3$

W. J. Ince

14 October 1965

Prepared for the Advanced Research Projects Agency
under Electronic Systems Division Contract AF 19(628)-5167 by

Lincoln Laboratory
MASSACHUSETTS INSTITUTE OF TECHNOLOGY
Lexington, Massachusetts

The work reported in this document was performed at Lincoln Laboratory, a center for research operated by Massachusetts Institute of Technology. This research is a part of Project DEFENDER, which is sponsored by the U.S. Advanced Research Projects Agency of the Department of Defense; it is supported by ARPA under Air Force Contract AF 19(628)-5167 (ARPA Order 498).

MASSACHUSETTS INSTITUTE OF TECHNOLOGY

LINCOLN LABORATORY

MAGNETIC STUDIES OF THE ANTIFERROMAGNET $RbMnF_3$

W. J. INCE

Group 44

TECHNICAL REPORT 384

14 OCTOBER 1965

LEXINGTON MASSACHUSETTS

MAGNETIC STUDIES OF THE ANTIFERROMAGNET $RbMnF_3$*

ABSTRACT

Magnetic properties of the antiferromagnet $RbMnF_3$ have been studied. Below T_N, the magnetic ions order into a two-sublattice system with the spins antiparallel. $RbMnF_3$ exhibits high exchange and low anisotropy; the form of the anisotropy surface is cubic. Consequently, for applied DC magnetic fields less than about 3000 oe, the static equilibrium position of the sublattice magnetization is, in general, multivalued.

Measurements of the DC susceptibility χ have been made on powder and single crystal specimens of $RbMnF_3$ for the range of applied field 0 to 12 koe and over the temperature range 4.2 to 300°K. The observed value of T_N was about ten degrees higher than the previously published value. When plotted as a function of applied field, $\chi_{[111]}$ shows no abrupt discontinuity analogous to the spin flopping exhibited by uniaxial antiferromagnets.

A simple model, in which H_{DC} and M are restricted to the (110) plane, has enabled solutions of the static equilibrium problem to be obtained. X-band resonance experiments are reported, and a resonance theory is presented which incorporates the equilibrium solutions. The predicted antiferromagnetic resonance spectrum shows reasonable agreement with the experimental data. The possibility of parallel pumping spin waves in $RbMnF_3$ is considered, and an attempt to measure the spin wave linewidth is described.

Accepted for the Air Force
Franklin C. Hudson
Chief, Lincoln Laboratory Office

---

*This report is based on a thesis of the same title submitted to the Department of Electrical Engineering at the Massachusetts Institute of Technology on 11 August 1965, in partial fulfillment of the requirements for the degree of Master of Science.

CONTENTS

Abstract iii

CHAPTER I – INTRODUCTION 1

CHAPTER II – DC SUSCEPTIBILITY MEASUREMENTS 5

A. General Discussion 5
B. Experimental Arrangement 6
C. Experimental Results 8
D. Discussion of Results 13

CHAPTER III – STATIC EQUILIBRIUM PROBLEM 15

A. The Model 15
B. Derivation of the Equilibrium Equation 16
C. Particular Equilibrium Solutions 18
D. Conclusions 20

CHAPTER IV – ANTIFERROMAGNETIC RESONANCE 21

A. Resonance Analysis 21
B. Normal Mode Frequencies for H_{DC} Parallel to a [111] Axis 25
C. Resonance Experiments 26
D. Experimental Results 27

CHAPTER V – EXCITATION OF SPIN WAVES BY PARALLEL PUMPING 33

A. Measurement of Spin Wave Linewidth by Parallel Pumping 33
B. Measurement Technique 37
C. Experimental Results 39

CHAPTER VI – CONCLUSIONS 41

APPENDIX – Derivation of the Transformation Matrix [T] 43

References 47

MAGNETIC STUDIES OF THE ANTIFERROMAGNET $RbMnF_3$

CHAPTER I
INTRODUCTION

This report describes certain aspects of the static and dynamic properties of $RbMnF_3$ – a perovskite material which has a simple cubic structure and is antiferromagnetic at temperatures less than 82.6°K. Below the Néel temperature, the Mn^{2+} ions order into a two-sublattice configuration with the magnetic moments antiparallel. According to published data,[1,2] $RbMnF_3$ exhibits low anisotropy and high exchange fields [356 and 7.08×10^7 amp/meter (4.47 and 8.9×10^5 oe), respectively]. Thus, antiferromagnetic resonance (AFMR) experiments can be performed without the need for extremely high DC magnetic fields and at convenient microwave frequencies (e.g., X-band). The form of the anisotropy appears to be entirely cubic, with no uniaxial component. The anisotropy constant is negative, so that the four cube diagonals are equivalent easy directions of magnetization.

Because $RbMnF_3$ is chemically quite stable, it is a very convenient material for general antiferromagnetic studies. It is possible to prepare relatively large single crystals which may be readily cut by conventional techniques. In the single crystal form, the material shows little or no tendency to absorb moisture.

The equilibrium position of the sublattice magnetizations under the action of an applied DC magnetic field, determined by minimizing the total free energy of the system, is not, in general, unique for an antiferromagnet that possesses cubic anisotropy. However, for sufficiently large values, the applied field and the magnetization will be almost orthogonal, regardless of the direction of the applied field with respect to the cube edges. In this case, the equilibrium position of the sublattice magnetizations is well defined. For $RbMnF_3$, experimental evidence shows that the perpendicular configuration is quite an accurate model for fields in excess of 8 koe. Freiser, et al.,[2] have performed a comprehensive investigation of AFMR for the high field case which has enabled them to investigate the anisotropy surface.

To the author's knowledge, no work has been published concerning the nature of the AFMR spectrum in $RbMnF_3$ in the low field region. For weak fields, Néel[3] has postulated the existence of domains in cubic antiferromagnets which, since the dipolar fields are small, are probably ill defined. Because of the likelihood of their existence, the resonance spectrum can be expected to be much more complicated.

Measurement of the DC magnetic susceptibility as a function of applied field for various crystal axes gives some insight into the equilibrium position of the magnetization. McGuire[4] has determined $\chi_{[100]}$ at 4.2°K and 1 koe by measuring the force on a single crystal of $RbMnF_3$

placed in a nonuniform magnetic field. He found $\chi_{[100]}$ to be $0.8\chi_{\perp}$ and concluded that the spins were distributed equally along the four cube diagonals. This simple picture cannot be correct, since the torque due to the applied field must, at least, rotate the magnetization vectors toward the [110] axis.

A study of the DC magnetic susceptibility was made using a vibrating sample magnetometer. The results are presented in Ch. II. Measurements at 4.2°K were made on a powder sample as well as on a single crystal. The results show that $\chi_{[100]}$ and $\chi_{[111]}$ are both increasing functions of H_{DC}, but approach an asymptotic value at about 8 koe. No effect was observed which corresponded to the abrupt spin flop transition of uniaxial antiferromagnets.[5]

Susceptibility measurements were also recorded as a function of temperature, from 4.2° to 300°K, enabling the Néel temperature and the exchange constants W_{11} and W_{12} to be determined.

Despite the complex nature of the problem concerning the static equilibrium position of the magnetization, the situation is considerably simplified if H_{DC} is restricted to lie in one of the crystal symmetry planes. A discussion of the static equilibrium is presented in Ch. III. The analysis, based on the molecular field approximation, assumes that the magnetization is uniform, i.e., the discussion is limited to a single domain, and that H_{DC} lies in a (110) plane. As expected, even for the restricted problem, the solution is multivalued.

A discussion of AFMR for a cubic material is presented in Ch. IV. Analysis of the linearized equations of motion yields two independent solutions for the resonant frequency of the system. The particular solutions obtained when H_{DC} is chosen to lie along a [111] axis are derived from an equation which is equivalent to the result obtained by Keffer and Kittel.[6]

X-band resonance data were obtained at five different frequencies. The resonances were studied in detail at 4.2°K as a function of angle and H_{DC}. Plots of H_{DC} required to excite resonance vs angle of applied field with respect to the cube edges indicate at least two resonances for each frequency. For at least two frequencies, many resonances are apparent which are clearly inexplicable on the basis of the simple theory. However, at least one resonant mode has been correlated as a function of frequency. Some of the characteristics of this mode can be predicted and are in agreement with the theory presented.

Spin wave instability and premature saturation of AFMR have been discussed by Heeger and Pincus.[7] The mechanism of spin wave growth and instability was first analyzed for the ferromagnetic case by Suhl.[8] He showed that such instabilities could be explained by a coupling of energy from the uniform precessional mode (spin wave number $k = 0$) to spin waves ($k \neq 0$) which are degenerate in energy with the uniform mode. The spin waves in turn couple energy to dissipative processes such as lattice vibrations. When the threshold driving field for the excitation of spin waves has been exceeded, the amplitude of the uniform precessional mode remains constant. Any further increase in incident power is coupled to the spin wave spectrum. The analysis by Heeger and Pincus for the antiferromagnetic case is similar. By considering the equations of motion for a two-sublattice system, they have calculated the critical field for the onset of instability and premature saturation of the AFMR.

The spin wave linewidth in $KMnF_3$, a material similar in structure to $RbMnF_3$, has been measured by Heeger.[9] He observed the apparent saturation of the susceptibility of the uniform mode at resonance and demonstrated that the critical field was anomalously low. The experimental data indicated that ΔH_k was about 5×10^{-3} oe, which is nearly four orders of magnitude less than the linewidth of the uniform precessional mode; ΔH_k was inferred from a measurement of the response of the resonant sample to amplitude modulated incident power.

Heeger's measurements indicate that the mechanisms responsible for the line broadening in spin wave excitation must be very different from those associated with the uniform mode for the material $KMnF_3$. The question arises whether $RbMnF_3$ exhibits similar behavior and whether the spin wave linewidth is the same order of magnitude. Chapter V describes a method and an experimental attempt to obtain ΔH_k in $RbMnF_3$ by measuring the threshold magnetic field for longitudinally pumped spin waves. The attractive feature of the so-called parallel pumping technique is that the uniform precessional mode is suppressed. This permits a more accurate measurement of spin wave linewidth, since the losses associated with the uniform precessional mode are absent. The result of the experiment was negative, which, however, was not interpreted as having set a lower limit to the value of ΔH_k. Analysis of the instability threshold makes the basic assumption that the pumping field is parallel to the magnetization and that the spin wave frequencies excited are very low. The negative result of this experiment, together with the results of the DC susceptibility and AFMR experiments, was taken to imply that these conditions were violated.

CHAPTER II
DC SUSCEPTIBILITY MEASUREMENTS

A. GENERAL DISCUSSION

The sublattice magnetizations of $RbMnF_3$ are quite well described by the Brillouin function for J = 5/2. The saturation magnetization M_S has been calculated from the formula, assuming a g-factor of two and the lattice constant equal to 4.24 Å, and was found to be* 3.04×10^5 amp/meter ($4\pi M_S$ equal to 3820 gauss).

According to the molecular field theory as applied to antiferromagnets, the fields acting on the respective sublattices are

$$H_1 = H_{DC} + W_{11}M_1 + W_{12}M_2$$

$$H_2 = H_{DC} + W_{22}M_2 + W_{21}M_1$$

where

$$W_{11} = W_{22}$$

and

$$W_{12} = W_{21} \quad .$$

The sum of the exchange constants W_{11} and W_{12}, defined by the above equation, may be evaluated from a plot of $1/\chi$ vs temperature within the paramagnetic region. The plot is a straight line of the form

$$\frac{1}{\chi} = T\left(\frac{1}{2C}\right) - \frac{1}{2}(W_{11} + W_{12})$$

where

$$C = \frac{n(P_{eff})^2 \mu_o}{3k} \qquad (1)$$

k is Boltzmann's constant, n is the number of Mn^{2+} ions per unit volume, and P_{eff} is the magnetic moment of the Mn^{2+} ion.

The straight line plot intercepts the negative temperature axis at a point given by

$$\Theta = C(W_{11} + W_{12}) \quad . \qquad (2)$$

The value of the slope and intercept enable $(W_{11} + W_{12})$ to be found; W_{11} and W_{12} may be completely determined from a measurement of the large field susceptibility, which is equal to $1/W_{12}$, below T_N. The magnitude of the slope of the line enables P_{eff}, whose value is well known,[10] to be verified. This provides one check of the accuracy of the measurements.

In addition to providing values of T_N, W_{11} and W_{12}, measurements of the DC susceptibility can give some insight into the equilibrium position of the magnetization.

---

* The quantum defect has not been taken into account.

A series of measurements of the magnetic susceptibility χ was made on powder and single crystal specimens of $RbMnF_3$.* The single crystal was cut so that it could be rotated about an axis perpendicular to the (110) plane. Measurements of χ with H_{DC} applied parallel to the [111] and [100] axes enabled two determinations of W_{11} and W_{12}. In the case of a powder, the density, which enters into the calculation for the exchange constants, is not well defined. Hence, the powder measurements were not used to determine W_{11} and W_{12}.

B. EXPERIMENTAL ARRANGEMENT

Magnetic susceptibility measurements were made using a vibrating sample magnetometer previously described by Hunt[11] and more recently modified by Santoro.[12] A block diagram of the instrument, which is modeled after Foner's design,[13] is shown in Fig. 1. The magnetometer measures the magnetic moment of a sample placed in a uniform magnetic field. The sample is made to vibrate in a direction perpendicular to the DC field by a voltage which is induced in a pair of stationary pickup coils that surround the sample. The vibrational motion of the sample

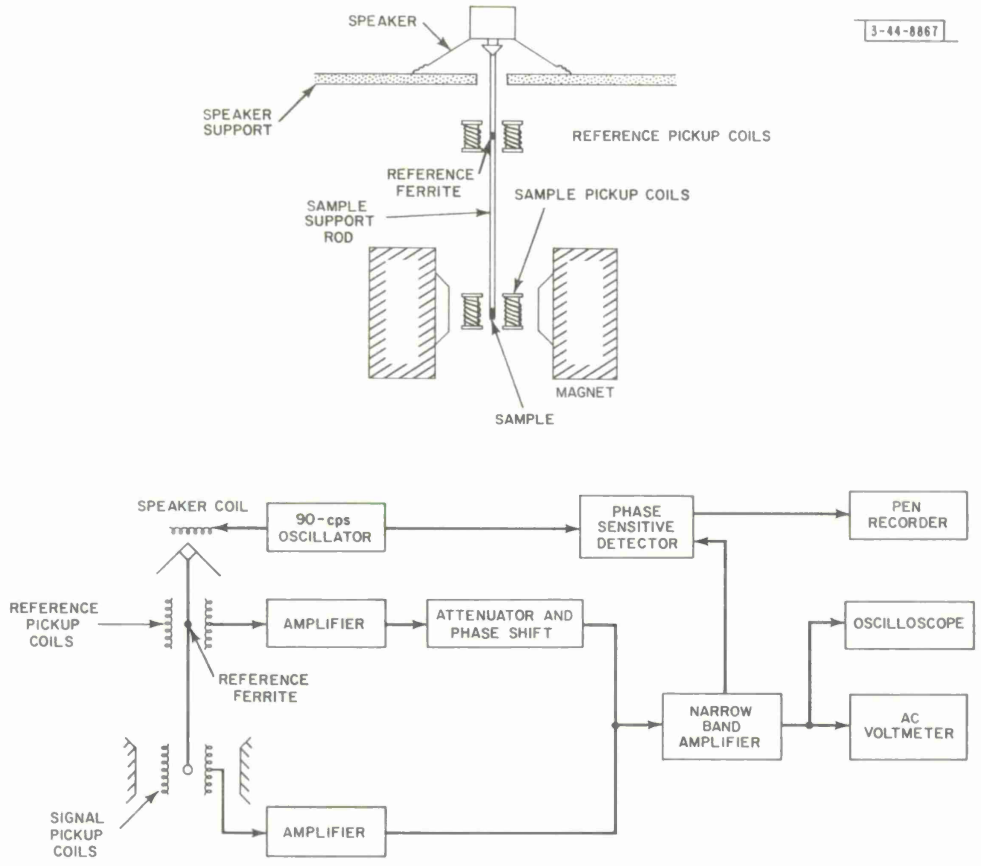

Fig. 1. Block diagram of magnetometer.

*All the $RbMnF_3$ samples used in this work were grown and donated by Dr. M. Kestigian of the Sperry Rand Research Center, Sudbury, Mass.

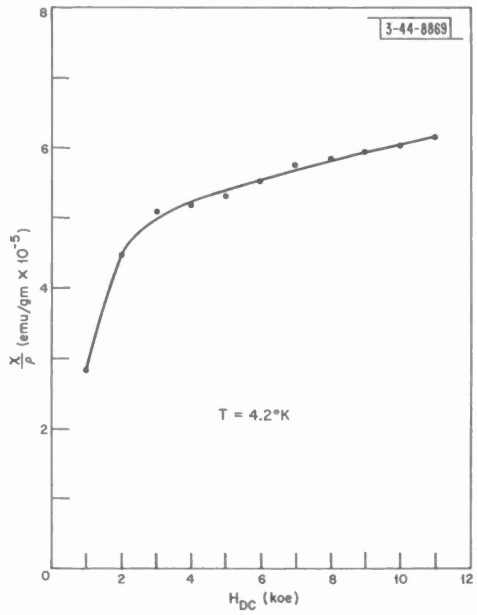

Fig. 2. χ/ρ vs H_{DC} for $RbMnF_3$ powder specimen.

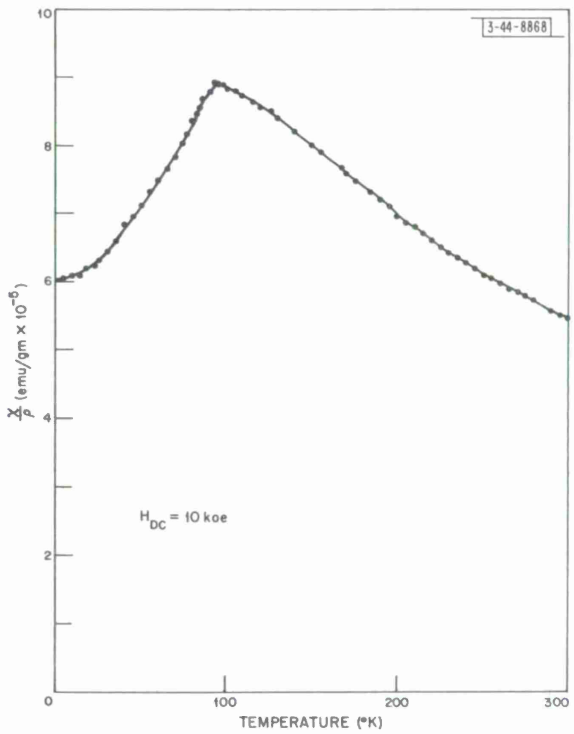

Fig. 3. χ/ρ vs temperature for $RbMnF_3$ powder specimen.

originates in a loud speaker cone. The sample is fastened to the end of a rod which is in turn rigidly attached to the cone. A second pair of pickup coils surrounds the upper part of the support rod. A small piece of ferrite attached to the rod at this point induces a reference voltage in the second pair. By the use of amplitude and phase adjustments, the signal and reference signals are balanced against each other, after appropriate amplification, to obtain a null condition. The magnetization per unit mass of the sample is then equal to RK/W, where K is a constant related only to the magnetometer, W is the weight of the sample, and R is the attenuator reading. The factor K is found experimentally by calibrating the instrument with a sample whose magnetization is known. The actual standard used was a nickel sphere (χ/ρ = 54.4 emu/gm at 300°K and is independent of applied field for $H_{DC} > 2$ koe).

The constant K is a function of sample position and the appropriate electromagnetic conversion factors. As a function of position, K(x, y, z) has a saddle point. It is necessary to locate the sample as near as possible to this point; otherwise, a slight displacement of the sample causes a change in the value of K. This is an important consideration in order to obtain good reproducibility of measurements and accuracy of calibration.

For the purpose of making susceptibility measurements as a function of temperature, the sample is cooled to liquid helium temperature and then allowed to return to room temperature over a period of several hours. Since there is little room between the pole pieces of the magnet, the magnetometer is equipped with a special narrow-necked dewar of somewhat limited capacity. The sample rod extends down into the dewar neck, and the helium is drawn up around the sample through a glass capillary tube that encases the sample rod and extends down into the body of the dewar vessel. The helium supply can maintain the sample at 4.2°K for about 10 minutes.

Temperature is measured by means of a copper constantan thermocouple. For the lowest temperatures, the liquid helium itself is used as the reference bath. As the sample warms and the helium in the reservoir becomes depleted, an ice bath is adopted as the reference.

C. EXPERIMENTAL RESULTS

The magnetic susceptibility per unit mass χ/ρ (ρ = density) of a powder specimen was measured as a function of DC magnetic field at 4.2°K over the range 1 to 11 koe. The results are plotted in Fig. 2. It can be seen that χ/ρ rises rapidly at first and then levels off at about 3 koe Above 3 koe, χ/ρ increases almost linearly, but at a much slower rate.

The susceptibility at 10 koe was measured as a function of temperature over the range 4.2° to 300°K. The results, shown in Fig. 3, clearly illustrate the Néel temperature. The susceptibility in the antiferromagnetic region follows the Van Vleck theory.[14] This indicates that although the sublattice magnetizations are antiparallel within each domain, the static equilibrium position of the magnetization vectors must be randomly distributed throughout the powder. The single crystal anisotropy is ineffective in determining the orientation of the sublattices with respect to H_{DC}. If it were effective, the spins would assume a position almost perpendicular to H_{DC} for a field as large as 10 koe, and χ/ρ would be fairly independent of temperature.

The considerable discrepancy between the measured value of T_N of 94°K and the previously published value[2] of 82.6°K was at first attributed to the fact that the thermocouple junction was not in direct contact with the powder sample. This source of error was later discounted because the same discrepancy was noted in the single crystal experiments in which it was possible to locate the junction much closer to the sample.

A plot of $(\chi/\rho)^{-1}$ vs temperature, shown in Fig. 4, yielded a straight line in the paramagnetic region. From the slope of the line and Eq. (1), P_{eff} was calculated to be 5.96 Bohr magnetons, which is in excellent agreement with the value of 5.92 quoted by Bates.[10]

The powder specimen, which weighed 0.82 gm, was prepared by grinding down a quantity of polycrystalline material and was sealed in a phenolic holder to prevent water absorption. Because of its size, not all the sample contributed fully to the magnetic moment. A correction factor was applied which was equivalent to using an effective mass, rather than the actual mass, in the susceptibility calculations. The correction factor was determined from a comparison with susceptibility data obtained from experiments with a single crystal sample which was much smaller (0.48 gm).

Figure 5 shows the variation of χ/ρ with H_{DC} for a single crystal oriented so that H_{DC} was applied along the [111] axis. The figure indicates a rapid increase in χ/ρ as H_{DC} is increased from 1 to 4 koe, followed by a gradual asymptotic leveling off to a value of 8.55×10^{-5} emu/gm.

$$\frac{1}{W_{12}} = 4\pi \times \text{Density} \times (\chi \text{ in emu/gm}) \quad .$$

Hence,

$$W_{12} = -216$$

and

$$H_E = |W_{12}| M_S = 216 \times 3.04 \times 10^5 = 6.56 \times 10^7 \text{ amp/meter}$$

$$(\text{or } 8.27 \times 10^5 \text{ oe}) \quad .$$

In Fig. 6, χ/ρ has been plotted as a function of temperature for the same crystal orientation. In the temperature range below T_N, two curves are shown corresponding to H_{DC} equal to 2 and 10 koe. The high field susceptibility, which is essentially equal to $\chi_\perp/\rho$, is constant up to a temperature of 80°K and then increases until T_N is reached. The low field susceptibility is equal to $0.765\,\chi_\perp/\rho$ at 4.2°K, climbs with temperature, and is roughly equal to $\chi_\perp/\rho$ at T_N. Clearly, in the low field case, all the magnetization cannot be along the easy axis parallel to H_{DC}; otherwise, the susceptibility at 4.2°K would be much smaller.

Figure 7 shows the variation of $(\chi/\rho)^{-1}$ with temperature. The value of P_{eff}, calculated from the slope of the curve in the paramagnetic region, is 5.96 Bohr magnetons. The negative temperature intercept is −160°K. From Eq. (2),

$$-160 = C(W_{11} + W_{12}) \quad .$$

Hence,

$$W_{11} + W_{12} = \underline{-238}$$

and therefore,

$$W_{11} = \underline{-22} \quad .$$

Curves of χ/ρ vs H_{DC}, χ/ρ vs temperature, and $(\chi/\rho)^{-1}$ vs temperature are shown in Figs. 8 through 10 for the case of H_{DC} parallel to a [100] axis. The same general trends are observed as for the previous orientation. The value of $|W_{12}|$, calculated from the large field

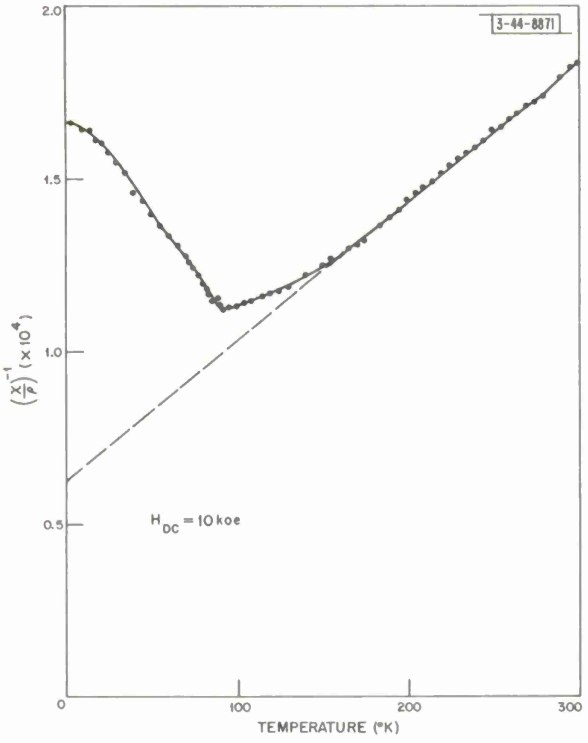

Fig. 4. $(\chi/\rho)^{-1}$ vs temperature for $RbMnF_3$ powder specimen.

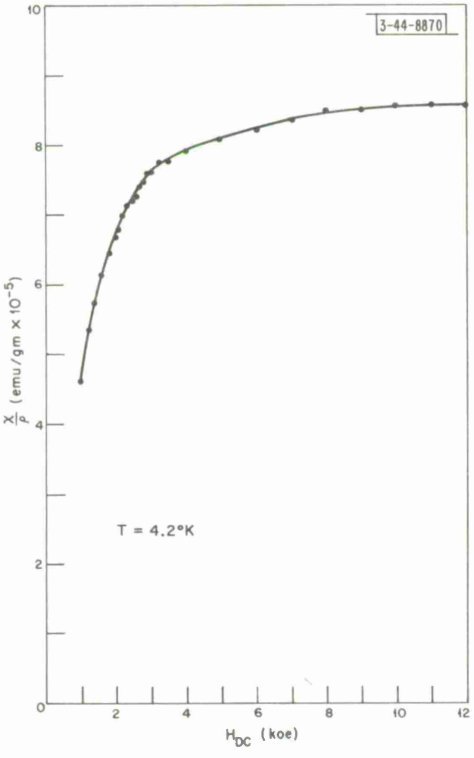

Fig. 5. χ/ρ vs H_{DC} for $RbMnF_3$ single crystal; H_{DC} parallel to [111] axis.

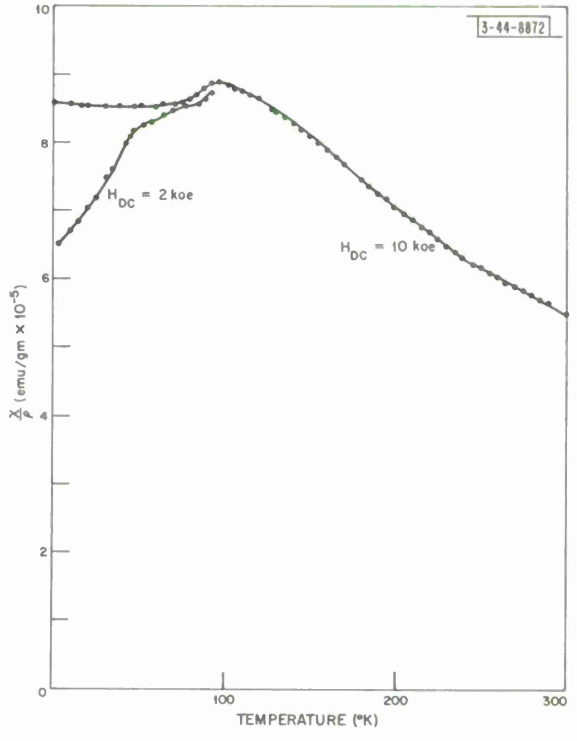

Fig. 6. χ/ρ vs temperature for $RbMnF_3$ single crystal; H_{DC} parallel to [111] axis.

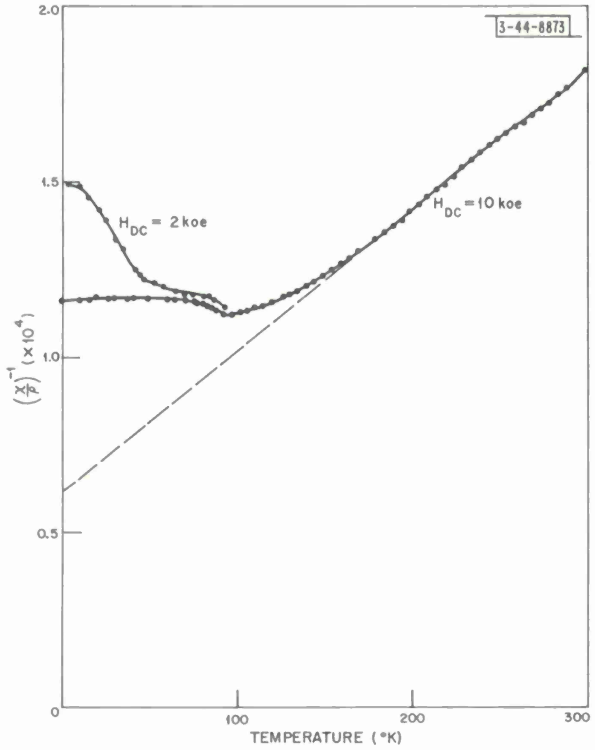

Fig. 7. $(\chi/\rho)^{-1}$ vs temperature for $RbMnF_3$ single crystal; H_{DC} parallel to [111] axis.

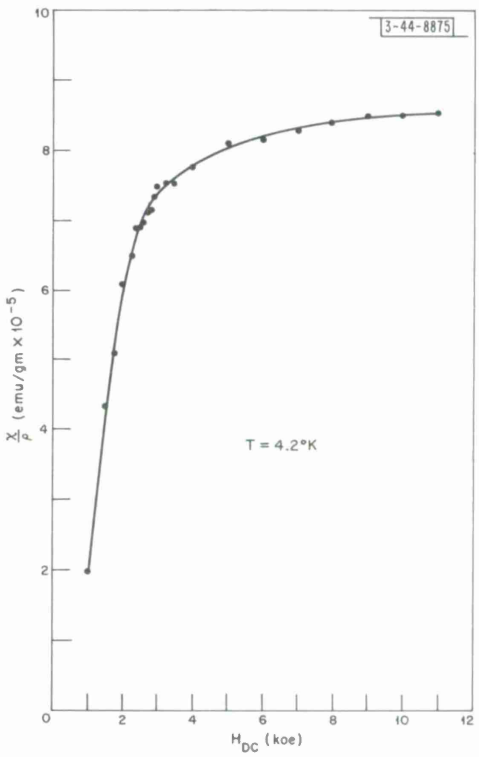

Fig. 8. χ/ρ vs H_{DC} for $RbMnF_3$ single crystal; H_{DC} parallel to [100] axis.

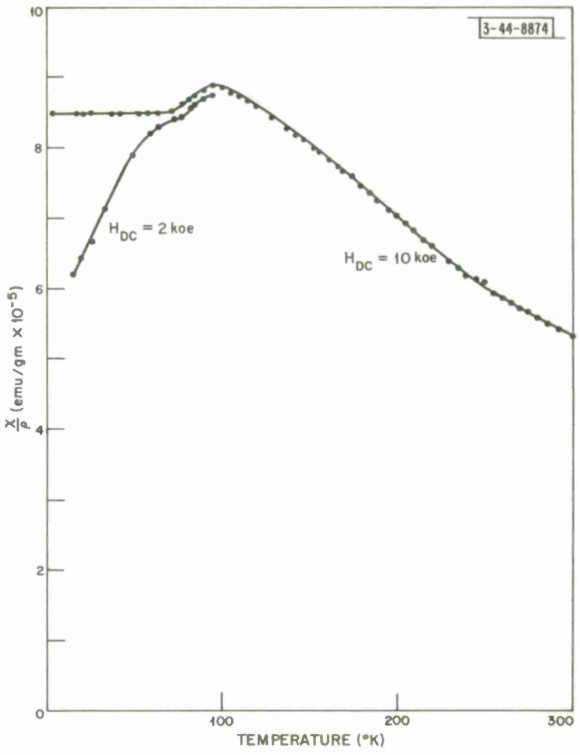

Fig. 9. χ/ρ vs temperature for $RbMnF_3$ single crystal; H_{DC} parallel to [100] axis.

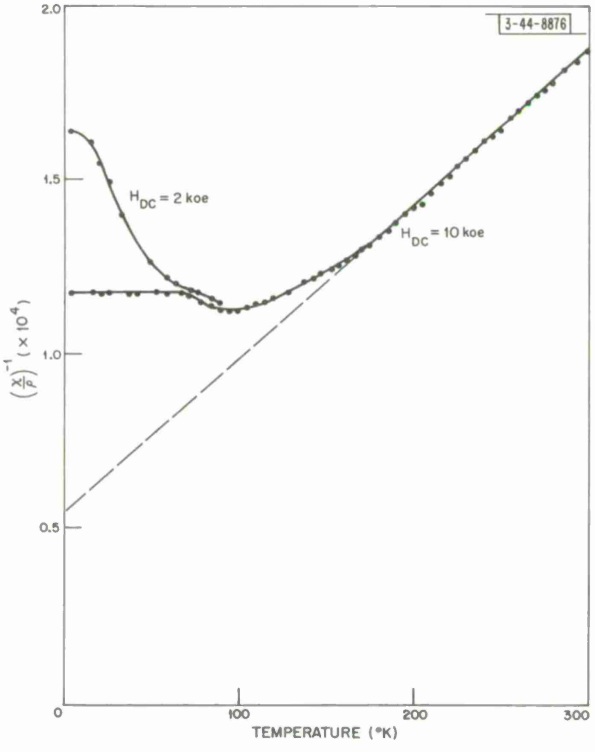

Fig. 10. $(\chi/\rho)^{-1}$ vs temperature for $RbMnF_3$ single crystal; H_{DC} parallel to [100] axis.

susceptibility at 4.2°K, is 216. The value of P_{eff}, calculated from the $(\chi/\rho)^{-1}$ vs temperature plot, is 5.8 Bohr magnetons, which is somewhat low. The negative temperature intercept is −192°K, giving a value of −80 for W_{11}.

D. DISCUSSION OF RESULTS

The measured value of T_N was about 94°K for both the single crystal and powder samples of $RbMnF_3$. This result is significantly different from the value reported by Freiser, et al.[2] Errors due to incorrect location of the thermocouple junction have already been discounted. The liquid nitrogen boiling point was checked for calibration purposes by first using the ice point and then the boiling point of liquid nitrogen for the reference temperature. In both cases, the calibration was within the accuracy (77.5 ± 1°K). During the experiment, the sample was cooled by a continual flow of gas rising from the evaporating coolant. Since the gas had low heat capacity, it is possible that conduction of heat along the thermocouple leads raised the junction temperature sufficiently to account for the discrepancy.

The absolute accuracy of the vibrating sample magnetometer ultimately relies on locating the sample exactly at the saddle point. The same precaution must be observed when calibrating the instrument with the nickel sphere. It was estimated that the absolute accuracy was not better than ±3 percent. The relative accuracy, i.e., repeatability of the measurements once the sample has been positioned at the saddle point, can be much less than 1 percent. However, considerable care must be taken to avoid the many sources of error. Common problems encountered were: (1) condensation of water vapor onto sample and capillary, (2) mechanical obstruction caused by the sample touching the capillary tube, (3) error signal induced in the pickup coil due to contact between the pickup coil and dewar vessel, (4) drift in the amplifiers due to fluctuating battery voltages.

There is excellent agreement between the calculated and published value of P_{eff} for the powder sample and for the single crystal with H_{DC} along the [111] axis. However, the calculated value of H_E and W_{12} are 7 percent lower than the value given by Freiser, et al.,[2] whereas the value of W_{11} is considerably lower (−22 compared to −95). It is important to note that W_{11} is calculated by taking the difference between two quantities fairly equal in magnitude, so that the above discrepancy is not surprising. The data calculated from the measurements with H_{DC} along the [100] axis are considered less reliable because of the low value of P_{eff}.

It has been shown[15] that for the Néel ground state to be stable,

$$\frac{W_{11}M_1}{W_{12}M_2} \text{ must be } > -\frac{1}{2} \quad .$$

For the two pairs of experimental values, $W_{11}/W_{12} < 1/2$. At 4.2°K, $M_1 = -M_2$. Hence, it follows that the stability criterion is satisfied. (Note that the value of T_N quoted in Ref. 1 would violate the criterion.)

The measurements of χ/ρ vs H_{DC} for the single crystal do not indicate any abrupt spin flopping over the entire range of applied field. The simple theory outlined in Ch. III predicts that flopping should occur for at least the [111] direction, provided M and H are in the same quadrant of the (110) plane, although misalignment of H_{DC} would reduce the effect (see Fig. 12).

CHAPTER III
STATIC EQUILIBRIUM PROBLEM

A. THE MODEL

The determination of the static equilibrium of the magnetization in a two-sublattice antiferromagnet is a four-variable problem. The variables may be taken to be the spherical position coordinates (Θ_i, φ_i), i = 1, 2, of each sublattice. The process of finding the equilibrium position involves minimizing the total free energy of the system. For a cubic antiferromagnet, this requires the solution of four inhomogeneous simultaneous transcendental equations. The result is, in general, multivalued. However, by restricting H_{DC} to lie in the (110) plane, the problem becomes much simpler. Despite the loss in generality, the restricted solution of the equilibrium problem is still very pertinent to the analysis of resonance experiments, particularly those reported in Ch. IV.

Figure 11 illustrates the directions of H_{DC} and the sublattice magnetizations in the (110) plane. The direction of H_{DC} makes an angle ψ with the [100] axis. The directions of M_1 and M_2 are Θ and $\Theta + \pi + \Delta\Theta$, respectively.

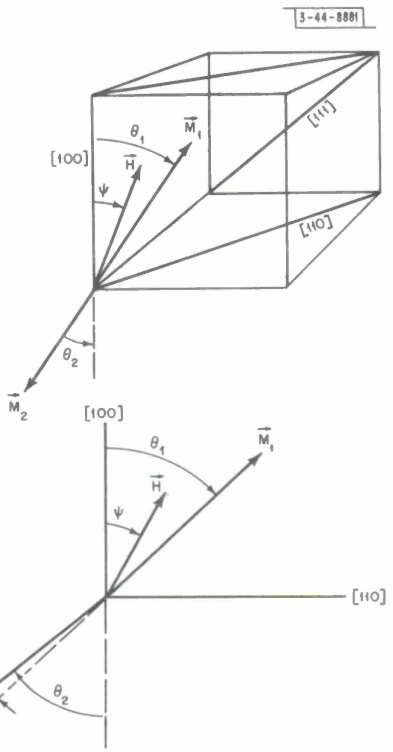

Fig. 11. Illustration of M and H_{DC} lying in the (110) plane.

The model is based on the assumption that the magnetization is locally uniform, i.e., a single domain is considered. A second assumption is that H_{DC}, M_1, and M_2 are coplanar. The statement is correct for certain directions of H_{DC} and is expected to hold for a range of ψ from symmetry considerations. The fact that the anisotropy surface is continuous and has a stationary value in the (110) plane indicates that the total energy can have a stationary value, which may or may not represent stable equilibrium. However, if these assumptions lead to a correct prediction of any of the observed microwave resonances, they will be justified.

B. DERIVATION OF THE EQUILIBRIUM EQUATION

The total free energy may be written as

$$\mathcal{H} = \mathcal{H}_{an} + \mathcal{H}_{ex} + \mathcal{H}_{Z}$$

where the subscripts refer to the anisotropy, exchange, and Zeeman energies, respectively.

$$\mathcal{H}_{an} = -\frac{K}{4}(\sin^4\theta_1 \sin^2 2\varphi_1 + \sin^2 2\theta_1 + \sin^4\theta_2 \sin^2 2\varphi_2 + \sin^2 2\theta_2)$$

where K is a positive constant.

$$\varphi_1 = \varphi_2 = \frac{\pi}{4} \quad , \quad \theta_1 = \theta \quad , \quad \theta_2 = \theta_1 + \pi + \Delta\theta \quad .$$

Hence,

$$\mathcal{H}_{an} = -\frac{K}{4}[\sin^4\theta + \sin^2 2\theta + \sin^4(\theta + \Delta\theta) + \sin^2(2\theta + 2\Delta\theta)] \quad .$$

The intersublattice exchange energy is

$$\mathcal{H}_{ex} = -\mu_o W_{12}\vec{M}_1 \cdot \vec{M}_2 - \frac{1}{2}\mu_o W_{11}|M_1|^2 - \frac{1}{2}\mu_o W_{22}|M_2|^2$$

where

$$M_1 = M = -M_2 \quad \text{and} \quad W_{11} = W_{22} \quad .$$

Assuming that the lengths of the vectors $\vec{M}_1$ and $\vec{M}_2$ remain fixed, the second two terms in $\mathcal{H}_{ex}$ do not enter into the minimizing of the total free energy with respect to the positions of M_1 and M_2 and can be dropped.

Thus,

$$\mathcal{H}_{ex} = -\mu_o W_{12}\vec{M}_1 \cdot \vec{M}_2 = \mu_o W_{12} M^2 \cos\Delta\theta$$

and

$$\mathcal{H}_{Z} = -\mu_o(\vec{M}_1 + \vec{M}_2) \cdot \vec{H}$$

$$= -\mu_o MH[\cos(\theta - \psi) - \cos(\theta + \Delta\theta - \psi)]$$

where H is the DC field.

Hence, the total energy is given by

$$\mathcal{H} = \mu_o W_{12} M^2 \cos\Delta\theta - \mu_o MH[\cos(\theta - \psi) - \cos(\theta + \Delta\theta - \psi)]$$

$$- \frac{K}{4}[\sin^4\theta + \sin^2 2\theta + \sin^4(\theta + \Delta\theta) + \sin^2 2(\theta + \Delta\theta)] \quad . \qquad (3)$$

By minimizing $\mathcal{H}$ with respect to $\Delta\theta$,

$$\frac{\partial\mathcal{H}}{\partial\Delta\theta} = 0$$

which, after some manipulation, becomes

$$[H_{ex} - H\cos(\theta - \psi)]\sin\Delta\theta = H\sin(\theta - \psi)\cos\Delta\theta + \frac{1}{8}\left(\frac{K}{\mu_o M}\right)[2\sin 2(\theta + \Delta\theta)$$

$$+ 3\sin 4(\theta + \Delta\theta)]$$

where

$$H_{ex} = |W_{12}|M \quad .$$

In conformity with the usual definition of effective anisotropy field,

$$\vec{H}_{an} = -\frac{1}{\mu_o}\frac{\partial \mathcal{H}_{an}}{\partial \vec{M}_i}$$

and $H_a = 4K/3\mu_o M$, where H_a is the effective anisotropy field along the [111] axis. By expanding the terms involving $\Delta\Theta$ and rearranging the equation,

$$\Delta\Theta = \frac{H \sin(\Theta - \psi) + \frac{3H_a}{32}(2 \sin 2\Theta + 3 \sin 4\Theta)}{H_{ex} - H \cos(\Theta - \psi) + \frac{3H_a}{8}(\cos 2\Theta - 3 \cos 4\Theta)} \quad .$$

We now examine the magnitude of the various quantities in the above expression. The largest value of H that will be considered is 10 koe. Since H_a and H_{ex} are 4.47 and 8.9×10^5 oe, respectively, there is clearly negligible error in the approximation:

$$\Delta\Theta \cong \frac{H \sin(\Theta - \psi)}{H_{ex}} \quad . \tag{4}$$

The term involving H in the denominator can be discarded because, if H is large, $\cos(\Theta - \psi) \cong 90°$. Hence, the term is always small. The above result shows that even for the largest value of H to be considered, $\Delta\Theta$ is only a fraction of a degree.

It is noted that Eq. (4) does not contain H_a explicitly. Hence, finding the equilibrium position first involves a trade-off between Zeeman and exchange energies, followed by a rotation of the magnetization to minimize the total energy.

By using the small angle approximations, $\sin\Delta\Theta \cong \Theta$ and $\cos\Delta\Theta = 1 - \frac{1}{2}(\Delta\Theta)^2$, and neglecting the effect of $\Delta\Theta$ on the anisotropy energy, Eq. (4) enables the total free energy equation to be written as

$$\frac{\mathcal{H}}{\mu_o M} = -H_{ex}\left[1 - \frac{1}{2}\left(\frac{H}{H_{ex}}\right)^2 \sin^2(\Theta - \psi)\right] - H\left\{\cos(\Theta - \psi)\left(\frac{H}{H_{ex}}\right)^2\left[\frac{\sin^2(\Theta - \psi)}{2}\right.\right.$$
$$\left.\left. + \left(\frac{H}{H_{ex}}\right)\sin^2(\Theta - \psi)\right]\right\} - \frac{3}{8} H_a(\sin^4\Theta + \sin^2 2\Theta) \quad . \tag{5}$$

By minimizing $\mathcal{H}$ with respect to Θ, $(1/\mu_o M)(\partial\mathcal{H}/\partial\Theta) = 0$, which leads to the result:

$$\frac{4H^2}{3H_{ex}H_a}\left\{\sin 2(\Theta - \psi) + \left(\frac{H}{2H_{ex}}\right)\sin(\Theta - \psi)[1 + 3\cos 2(\Theta - \psi)]\right\} = -\sin 2\Theta(1 + 3\cos 2\Theta) \quad . \tag{6}$$

The second term on the left side of Eq. (6) is quite negligible compared to the first term, since $H/H_{ex} = 1/100$, except in the pathological case of $\sin 2(\Theta - \psi) = 0$. Even for this case, the resulting error in Θ is small. Hence, the final expression for the equilibrium is

$$\frac{4H^2}{3H_{ex}H_a}\sin 2(\Theta - \psi) = -\sin 2\Theta(1 + 3\cos 2\Theta) \tag{7}$$

and the total free energy at equilibrium is given by

$$\frac{\mathcal{H}}{\mu_o M} = -H_{ex} - \frac{H^2}{H_{ex}} \sin^2(\theta - \psi) - \frac{H^3}{2H_{ex}^2} \sin^2(\theta - \psi) \cos(\theta - \psi)$$

$$- \frac{3}{8} H_a(\sin^4\theta + \sin^2 2\theta) \quad . \tag{8}$$

Whether the equilibrium is stable or unstable may be determined by examining the second derivative of the energy and finding whether it is positive or negative. After differentiating and simplifying,

$$\frac{1}{\mu_o M} \frac{\partial^2 \mathcal{H}}{\partial \theta^2} = - \frac{H^2}{H_{ex}} \cos 2(\theta - \psi) - \frac{H^3}{2H_{ex}^2} \cos(\theta - \psi) [2 - 9 \sin^2(\theta - \psi)]$$

$$- \frac{3}{4} H_a (\cos 2\theta + 3 \cos 4\theta) \quad . \tag{9}$$

C. PARTICULAR EQUILIBRIUM SOLUTIONS

Case 1: H = 0

Equation (7) reduces to $\sin 2\theta (1 + 3 \cos 2\theta) = 0$. Hence, either

$$\sin 2\theta = 0 \quad , \quad \text{i.e., } \theta = (2n + 1) \frac{\pi}{2}$$

or

$$\cos 2\theta = - \frac{1}{3} \quad , \quad \text{i.e., } \theta = \pm 54.7^\circ \quad \text{or} \quad \pm(180^\circ - 54.7^\circ) \quad .$$

For $\theta = [(2n + 1)\pi]/2$, Eq. (9) shows that these are unstable equilibria. The solutions represent the magnetization along the cube edges, which are the hard directions.

The solutions for which $\cos 2\theta = -(1/3)$ represent the four <111> axes. Equation (9) shows that these are stable equilibria.

Case 2: H Along a ⟨111⟩ Direction ($\psi = 54.7^\circ$)

Unless H = 0, as already discussed, $\sin 2\theta = 0$ is no longer a solution. Two solutions exist: either

$$\sin 2(\theta - \psi) = 0 \quad \underline{\text{and}} \quad (1 + 3 \cos 2\theta) = 0$$

or

$$\frac{4H^2}{3H_{ex}H_a} \sin 2(\theta - \psi) = - \sin 2\theta (1 + 3 \cos 2\theta) \quad .$$

The first solution corresponds to the spins lying along the [111] axis and parallel to H. Substitution of the constraint $\theta = \psi = 54.7^\circ$ into Eq. (9) gives the condition

$$\frac{1}{\mu_o M} \frac{\partial^2 \mathcal{H}}{\partial \theta^2} = - \frac{H^2}{H_{ex}} - \frac{H^3}{H_{ex}^2} + 2H_a > 0$$

for stability. By neglecting the second term, $H^2 < 2H_{ex}H_a$.

For the second solution, when H = 0, $\theta = (180^\circ - 54.7^\circ)$; and when $H = \infty$, $\theta = (90^\circ + \psi)$, i.e., the spins are orthogonal to H. It follows that $125.3^\circ \leqslant \theta \leqslant 144.7^\circ$. From this inequality, it can be shown that the second solution always represents a stable equilibrium.

Hence, as H is increased from zero strength, any spins initially directed along the [111] axis parallel to H will remain there until H exceeds the value $\sqrt{2H_{ex}H_a}$. The only other stable equilibrium position is then at an angle lying between 125.3° and 144.7°, and the magnetization will suddenly rotate, or flop, to the new position. This is analogous to the spin flopping in a uniaxial antiferromagnet. There is, however, an important difference. The spins will not flop back when H is reduced again, but will slowly rotate. At zero field, the spins will point in the direction $\Theta = 125.3°$, i.e., along the other [111] axis in the (110) plane. According to the simple theory, at least 25 percent of the magnetization will initially point in the latter direction. These spins will never flop, but will rotate slowly under the action of varying field strength as outlined above.

Case 3: H Along a ⟨100⟩ Direction ($\psi = 0$)

Solutions to Eq. (7) are

$$\sin 2\Theta = 0 \quad , \quad \text{i.e.,} \quad \Theta = (2n + 1)\frac{\pi}{2}$$

or

$$\frac{4H^2}{3H_{ex}H_a} = -(1 + 3\cos 2\Theta) \quad .$$

The solution, $\sin 2\Theta = 0$, is stable if $H^2 > 3H_{ex}H_a/2$.

The second solution becomes imaginary if $H^2 > 3H_{ex}H_a/2$,. but for lower values of H, it is the only solution and is stable.

Case 4: H Along a ⟨110⟩ Direction ($\psi = 90°$)

Equation (7) becomes

$$\frac{4H^2}{3H_{ex}H_a}\sin 2\Theta = \sin 2\Theta(1 + 3\cos 2\Theta) \quad .$$

The two solutions are either

$$\sin 2\Theta = 0 \quad , \quad \text{i.e.,} \quad \Theta = n\pi$$

or

$$\frac{4H^2}{3H_{ex}H_a} = 1 + 3\cos 2\Theta \quad .$$

The first solution is stable if $H^2 > 3H_{ex}H_a$.

The second solution does not exist if $H^2 > 3H_{ex}H_a$, because $\cos 2\Theta$ is greater than unity. For the second solution to be stable,

$$\left(\frac{H^2}{H_{ex}} - \frac{3H_a}{4}\right)\cos 2\Theta - \frac{9H_a}{4}\cos 4\Theta > 0 \quad .$$

The inadequacy of the model may be noted by considering the effect of a strong field applied along a ⟨110⟩ direction. The above result states that the magnetization will be perpendicular to H and directed along the [100] axis. However, the [100] axis is a hard axis, and the spins are free to rotate out of the (110) plane that contains H, while maintaining the orthogonality condition with respect to H, until they lie along the [110] direction. Clearly, this is a lower energy state.

Case 5: H in an Arbitrary Direction

For the general case, the transcendental Eq. (7) must be solved, and the solution must then be checked for stability. This was done for five values of ψ. The results are shown in Fig. 12. The dotted portions of the curves for $\psi = 10°$ and $\psi = 45°$ represent unstable regions.

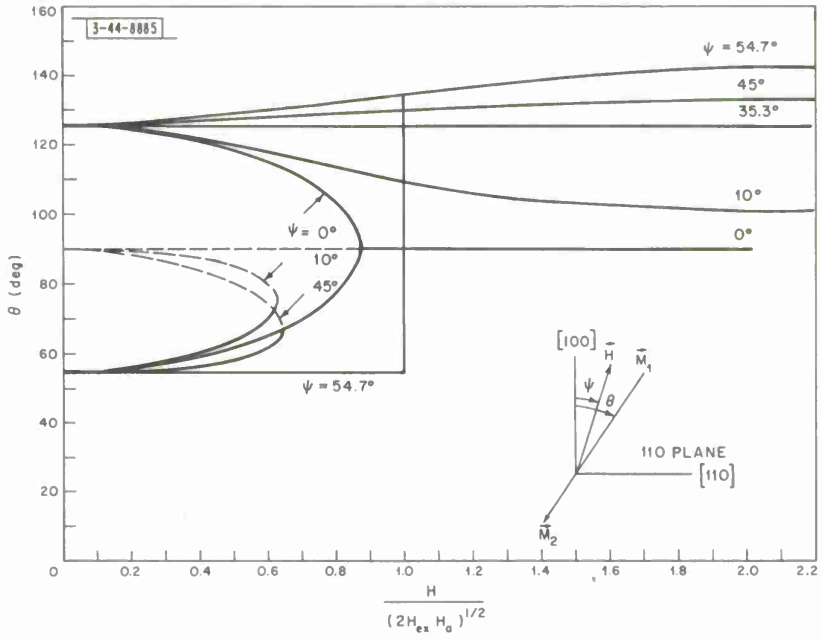

Fig. 12. Equilibrium position of sublattice magnetizations as a function of H_{DC}.

D. CONCLUSIONS

The model enables a simple expression for the equilibrium position of the magnetization to be found. It appears to give reasonable solutions for H parallel to the [100] and [111] axes, but leads to a contradictory result for a large field applied along a [110] axis.

The magnetic field acts differently on the magnetization depending on whether M and H are in the same quadrant of the {110} plane or in different quadrants. For the latter case, as H is increased, the magnetization rotates away from H. For very large fields, M and H are perpendicular. If M and H are initially in the same quadrant, with H along the [111] axis, M will keep its orientation along the same [111] axis until H exceeds a certain value, equal to $\sqrt{2H_{ex}H_a}$, when M will abruptly flop into the adjacent quadrant. If M and H are initially in the same quadrant and H is not along the [111] axis, M gradually rotates away from H as it is increased. After a certain rotation, depending on the magnitude and orientation of H, M will flop into the adjacent quadrant and remain there.

The simple model predicts that under the action of a DC magnetic field, a single crystal of $RbMnF_3$ can act like a two-state device. If a strong field is applied to one quadrant in the (110) plane, it will cause any magnetization lying along an axis within that quadrant to rotate into the adjacent quadrant in the plane and remain there when the field is removed. If the field is then applied within the quadrant to which M rotated, it will cause M to rotate back to its original quadrant and remain there.

CHAPTER IV
ANTIFERROMAGNETIC RESONANCE

A. RESONANCE ANALYSIS

The equation of motion for the two-sublattice antiferromagnet is

$$\frac{1}{\gamma}(\dot{\vec{M}}_i + \delta\dot{\vec{M}}_i) = \mu_o(\vec{M}_i + \delta\vec{M}_i) \times [\vec{H}_{oi} + W_{ii}(\vec{M}_i + \delta\vec{M}_i) + W_{ij}(\vec{M}_j + \delta\vec{M}_j)] + \vec{T}_i + \delta\vec{T}_i$$

$$i,j = 1,2 \quad \text{and} \quad i \neq j \quad .$$

The capital letters represent the steady state values, the deltas refer to increments about the equilibrium position, and $\vec{T}$ represents the torque resulting from the anisotropy energy. Demagnetizing effects are neglected.

$\vec{H}_{oi} = \vec{H}_{DC} + \vec{H}_{Ni}$, where $\vec{H}_{Ni}$ is the nuclear hyperfine field[2] and acts in the direction of $\vec{M}_i$. The nuclear hyperfine interaction is important for $RbMnF_3$, since at low temperatures, it is comparable in magnitude [(= 9.46/T°K) oe] to the effective crystalline anisotropy field. The terms that contribute to the static equilibrium condition may be separated from the dynamic terms:

$$\frac{\dot{\vec{M}}_i}{\gamma} = 0 = \mu_o\vec{M}_i \times (\vec{H}_{oi} + W_{ii}\vec{M}_i + W_{ij}\vec{M}_j) + \vec{T}_i \quad .$$

Therefore,

$$\frac{\delta\dot{\vec{M}}_i}{\gamma} = \mu_o[\delta\vec{M}_i \times (\vec{H}_{oi} + W_{ij}\vec{M}_j) + \vec{M}_i \times W_{ij}\delta\vec{M}_j] + \delta\vec{T}_i \quad . \tag{10}$$

The anisotropy energy for the two-sublattice cubic system can be expressed as

$$\mathcal{H}_{an} = -\frac{K}{M^4}(M_{1x}^2M_{1y}^2 + M_{1x}^2M_{1z}^2 + M_{1y}^2M_{1z}^2 + M_{2x}^2M_{2y}^2 + M_{2x}^2M_{2z}^2 + M_{2y}^2M_{2z}^2)$$

and

$$\vec{H}_{ai_{x,y}} = -\frac{1}{\mu_o}\frac{\partial\mathcal{H}}{\partial\vec{M}_{i_{x,y}}}$$

neglecting intersublattice anisotropy. The anisotropy torques are found by taking the vector product $\vec{M}_i \times \vec{H}_{ai}$. Assuming that the axes of the Cartesian coordinate system are chosen to coincide with the cube edges,

$$T_{ix} = M_{iy}H_{aiz} - M_{iz}H_{aiy} = \frac{2K}{M^4}M_{iy}M_{iz}(M_{iy}^2 - M_{iz}^2)$$

$$T_{iy} = M_{iz}H_{aix} - M_{ix}H_{iz} = \frac{2K}{M^4}M_{ix}M_{iz}(M_{iz}^2 - M_{ix}^2)$$

$$T_{iz} = M_{ix}H_{aiy} - M_{iy}H_{ix} = \frac{2K}{M^4}M_{ix}M_{iy}(M_{ix}^2 - M_{iy}^2) \quad .$$

Hence,

$$T_{ix} + \delta T_{ix} = \frac{2K}{M^4}(M_{iy} + \delta M_{iy})(M_{iz} + \delta M_{iz})[(M_{iy} + \delta M_{iy})^2 - (M_{iz} + \delta M_{iz})^2] \quad .$$

$$[A] = \begin{bmatrix} 0 & (H_{o1z} + W_{12}M_{2z}) & -(H_{o1y} + W_{12}M_{2y}) & 0 & -W_{12}M_{1z} & W_{12}M_{1y} \\ -(H_{o1z} + W_{12}M_{2z}) & 0 & (H_{o1x} + W_{12}M_{2x}) & W_{12}M_{1z} & 0 & -W_{12}M_{1x} \\ (H_{o1y} + W_{12}M_{2y}) & -(H_{o1x} + W_{12}M_{2x}) & 0 & -W_{12}M_{1y} & W_{12}M_{1x} & 0 \\ 0 & -W_{12}M_{2z} & W_{12}M_{2y} & 0 & (H_{o2z} + W_{12}M_{1z}) & -(H_{o2y} + W_{12}M_{1y}) \\ W_{12}M_{2z} & 0 & -W_{12}M_{2x} & -(H_{o2z} + W_{12}M_{1z}) & 0 & (H_{o2x} + W_{12}M_{1x}) \\ -W_{12}M_{2y} & W_{12}M_{2x} & 0 & (H_{o2y} + W_{12}M_{1y}) & -(H_{o2x} + W_{12}M_{1x}) & 0 \end{bmatrix}$$

$$[B] = \frac{1}{\mu_o} \begin{bmatrix} 0 & \frac{2K}{M^4}(3M_{1z}M_{1y}^2 - M_{1z}^3) & -\frac{2K}{M^4}(3M_{1z}^2M_{1y} - M_{1y}^3) & 0 & 0 & 0 \\ -\frac{2K}{M^4}(3M_{1x}^2M_{1z} - M_{1z}^3) & 0 & \frac{2K}{M^4}(3M_{1z}^2M_{1x} - M_{1x}^3) & 0 & 0 & 0 \\ \frac{2K}{M^4}(3M_{1x}^2M_{1y} - M_{1y}^3) & -\frac{2K}{M^4}(3M_{1y}^2M_{1x} - M_{1x}^3) & 0 & 0 & 0 & 0 \\ 0 & 0 & 0 & 0 & \frac{2K}{M^4}(3M_{2z}M_{2y}^2 - M_{2z}^3) & -\frac{2K}{M^4}(3M_{2z}^2M_{2y} - M_{2y}^3) \\ 0 & 0 & 0 & -\frac{2K}{M^4}(3M_{2x}^2M_{2z} - M_{2z}^3) & 0 & \frac{2K}{M^4}(3M_{2z}^2M_{2x} - M_{2x}^3) \\ 0 & 0 & 0 & \frac{2K}{M^4}(3M_{2x}^2M_{2y} - M_{2y}^3) & -\frac{2K}{M^4}(3M_{2y}^2M_{2x} - M_{2x}^3) & 0 \end{bmatrix}$$

It follows that

$$\delta T_{ix} = \frac{2K}{M^4} [\delta M_{iy}(3M_{iz}M_{iy}^2 - M_{iz}^3) - \delta M_{iz}(3M_{iz}^2 M_{iy} - M_{iy}^3)] \quad .$$

Similarly,

$$\delta T_{iy} = \frac{2K}{M^4} [\delta M_{iz}(3M_{iz}^2 M_{ix} - M_{ix}^3) - \delta M_{ix}(3M_{ix}^2 M_{iz} - M_{iz}^3)]$$

and

$$\delta T_{iz} = \frac{2K}{M^4} [\delta M_{ix}(3M_{ix}^2 M_{iy} - M_{iy}^3) - \delta M_{iy}(3M_{iy}^2 M_{ix} - M_{ix}^3)] \quad .$$

Equation (10) is now linearized and written in terms of Cartesian components. Six simultaneous equations are obtained; the variables are the six differential increments δM_{ix}, δM_{iy}, δM_{iz}. In matrix notation, the set of equations may be written as

$$\frac{j\omega}{\gamma\mu_o} [\delta M] = [A] [\delta M] + [B] [\delta M] \quad . \tag{11}$$

Matrix [A] contains the coefficients of δM which are invariant to a rotation of the coordinates; [B] contains the anisotropic terms which are affected by a rotation.

The coordinates are now rotated through an angle Θ in the (110) plane so that the new z-axis and the equilibrium direction of the magnetization coincide. The new coordinates will be referred to as (x,y,z). Thus, $M_z = M$, and $M_x = M_y = 0$.

If [T] is the transformation matrix from the new to the old axes $[\delta M] = [T] [\delta m]$, where $[\delta m]$ represents the dynamic components of the magnetization in the new coordinate system. Hence, from Eq. (11),

$$\frac{j\omega}{\gamma} [\delta m] = [A] [\delta m] + [T]^{-1} [B] [T] [\delta m]$$

where the components in [A] are written in terms of the new coordinates. The equation

$$\frac{j\omega}{\gamma} [\delta m] = [a] [\delta m] + [b] [\delta m] \tag{12}$$

defines the new matrices [a] and [b].

The derivation of the transformation matrix is given in the Appendix. For the two-sublattice system, it becomes a 6×6 matrix:

$$[T] = \begin{bmatrix} \left(\frac{\cos\theta + 1}{2}\right) & \left(\frac{\cos\theta - 1}{2}\right) & \frac{\sin\theta}{\sqrt{2}} & 0 & 0 & 0 \\ \left(\frac{\cos\theta - 1}{2}\right) & \left(\frac{\cos\theta + 1}{2}\right) & \frac{\sin\theta}{\sqrt{2}} & 0 & 0 & 0 \\ \frac{-\sin\theta}{\sqrt{2}} & \frac{-\sin\theta}{\sqrt{2}} & \cos\theta & 0 & 0 & 0 \\ 0 & 0 & 0 & \left(\frac{\cos\theta + 1}{2}\right) & \left(\frac{\cos\theta - 1}{2}\right) & \frac{\sin\theta}{\sqrt{2}} \\ 0 & 0 & 0 & \left(\frac{\cos\theta - 1}{2}\right) & \left(\frac{\cos\theta + 1}{2}\right) & \frac{\sin\theta}{\sqrt{2}} \\ 0 & 0 & 0 & \frac{-\sin\theta}{\sqrt{2}} & \frac{-\sin\theta}{\sqrt{2}} & \cos\theta \end{bmatrix}$$

and

$$[T]^{-1} = [T]^{t} \quad .$$

By invoking the constraint that the total magnetization must be conserved, [a] and [b] may be reduced from 6×6 to 4×4 matrices.

$$m_1^2 = M^2 = (m_{1x} + \delta m_{1x})^2 + (m_{1y} + \delta m_{1y})^2 + (m_{1z} + \delta m_{1z})^2 \quad .$$

Putting

$$m_{1x}^2 + m_{1y}^2 + m_{1z}^2 \cong M^2$$

and neglecting the second order terms

$$m_{1x}\delta m_{1x} + m_{1y}\delta m_{1y} + m_{1z}\delta m_{1z} = 0 \quad .$$

Since $m_{1x} = m_{1y} = 0$, and $m_{1z} \neq 0$, it follows that $\delta m_{1z} = 0$. Similarly, $\delta m_{2z} = 0$. Hence, the rows and columns in [a] and [b] associated with δm_{1z} and δm_{2z} may be struck out.

After considerable algebraic work,

$$[a] = \begin{bmatrix} 0 & (H_{DCz} + H_N + H_{ex}) & 0 & H_{ex} \\ -(H_{DCz} + H_N + H_{ex}) & 0 & -H_{ex} & 0 \\ 0 & -H_{ex} & 0 & (H_{DCz} - H_N - H_{ex}) \\ H_{ex} & 0 & -(H_{DCz} - H_N - H_{ex}) & 0 \end{bmatrix}$$

$$[b] = \begin{bmatrix} b_{11} & b_{12} & 0 & 0 \\ -b_{12} & -b_{11} & 0 & 0 \\ 0 & 0 & -b_{11} & -b_{12} \\ 0 & 0 & b_{12} & b_{11} \end{bmatrix}$$

and

$$b_{11} = \frac{3K}{\mu_o M} \sin^2\Theta \left(\cos^2\Theta - \frac{\sin^2\Theta}{2}\right)$$

$$b_{12} = \frac{2K}{\mu_o M} \left(3 \sin^2\Theta \cos^2\Theta - \cos^4\Theta + \frac{\sin^4\Theta}{4}\right) \quad .$$

Equation (12) is rewritten as

$$[a + b - \frac{j\omega}{\gamma}] [\delta m] = 0 \quad \text{or} \quad [c] [\delta m] = 0 \quad .$$

The determinant of [c] must be equal to zero for the set of linear equations to be simultaneously true. By multiplying out the determinant, a biquadratic equation results in ω/γ:

$$D(\frac{\omega}{\gamma\mu_o})^4 + E(\frac{\omega}{\gamma\mu_o})^2 + F = 0$$

where D, E, and F are functions of the elements of [a] and [b].

Hence,

$$(\frac{\omega}{\gamma\mu_o})^2 = \frac{-E \pm \sqrt{E^2 - 4DF}}{2} \quad .$$

After the appropriate substitutions for D, E, and F and considerable algebra, the following expression for the normal mode resonant frequencies is obtained.

$$(\frac{\omega}{\gamma\mu_o})^2 = H_{DCz}^2 + 2H_{ex}(H_N + b_{12}) + (H_N + b_{12})^2 - b_{11}^2$$

$$\pm 2H_{DCz} \sqrt{2H_{ex}(H_N + b_{12}) + (H_N + b_{12})^2 + \left(\frac{b_{11} H_{ex}}{H_{DCz}}\right)^2} \quad . \qquad (13)$$

The equation yields only two independent frequencies. It is interesting to note that ω is independent of H_{DCx} and H_{DCy}. It is only a function of the component of H_{DC} along the equilibrium position of M.

B. NORMAL MODE FREQUENCIES FOR H_{DC} PARALLEL TO A [111] AXIS

For this important case, $b_{11} = 0$, and $b_{12} = H_a$. Equation (13) becomes a perfect square:

$$\left(\frac{\omega}{\gamma\mu_o}\right)^2 = \left\{H_{DCz} \pm \left[2H_{ex}(H_N + H_a) + (H_N + H_a)^2\right]^{1/2}\right\}^2$$

or

$$\frac{\omega}{\gamma\mu_o} = H_{DC}\cos(\Theta - \psi) \pm \sqrt{(H_N + H_a)(2H_{ex} + H_N + H_a)} \quad . \tag{14}$$

Now, if $H_{DC} < \sqrt{2H_{ex}H_a}$, one of the permitted equilibrium conditions is $\Theta = \psi = 54.7°$. Then Eq. (14) is equivalent to the well-known result of Keffer and Kittel.[6] However, there is another pair of frequencies that corresponds to the magnetization which was initially directed along the second [111] axis (not parallel to H_{DC}). The resonant frequencies for both pairs of modes have been plotted as a function of H_{DC} in Fig. 13. The low frequency branch should approach zero frequency at the spin flop field. The simple theory has neglected the nuclear magnetic resonance (NMR) modes which exist at much lower frequencies than the electronic modes. At low frequencies, the electronic and nuclear spin systems will couple in such a way that one branch of the coupled mode spectrum will go to zero frequency at the spin flopping field.

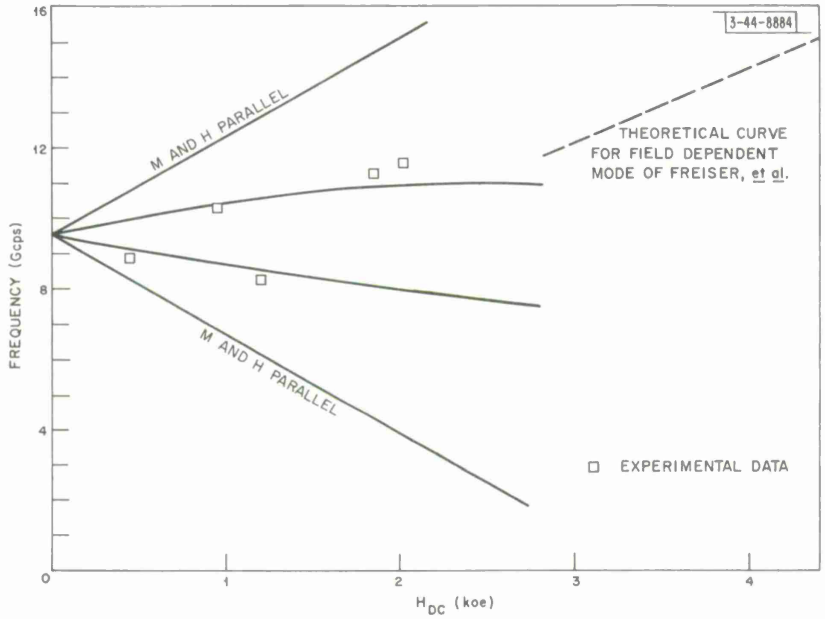

Fig. 13. AFMR in $RbMnF_3$; H_{DC} parallel to [111] axis.

C. RESONANCE EXPERIMENTS

Resonance experiments were performed at X-band and at 4.2°K with the experimental arrangement illustrated in the block diagram of Fig. 14. The single crystal $RbMnF_3$ specimen was a 4-mm cube which was cut so that four of its faces were (110) planes and two were (100) planes. The crystal was mounted in a TE_{10x} cavity at a point of maximum RF magnetic field and could be rotated about a [110] axis. Three different cavities were used so that experiments could be performed at five frequencies distributed over the X-band spectrum. The cavity and connecting waveguide were immersed in liquid helium. A glass double dewar system enabled the sample to be maintained at 4.2°K for many hours at a time. The dewar system was suspended between the pole pieces of a 12-inch Varian electromagnet. The waveguide and cavity were positioned so that the RF magnetic field at the crystal and H_{DC} were orthogonal. Rotation

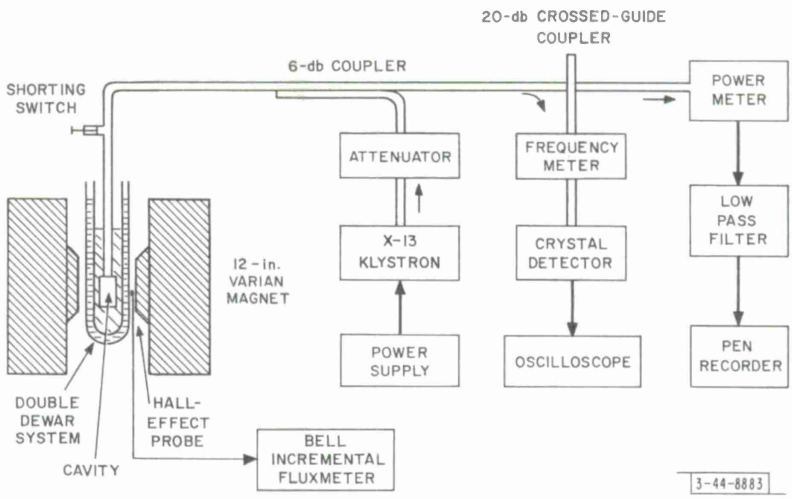

Fig. 14. Block diagram of X-band AFMR experimental arrangement.

of the crystal, which permitted the orientation of H_{DC} with respect to the cubic lattice to be varied during the experiment, was obtained through a gear train mounted on the end of the cavity. A shaft rotation was translated to the sample mount inside the cavity by a thin dielectric rod. It was necessary to evacuate the waveguide and dewar vessel, and refill it with gaseous helium before transferring liquid helium, in order to prevent the gear train from sticking.

Each of the cavities was of the reflection type and, by appropriate choice of iris, was arranged to be overcoupled at 4.2°K. Resonance was detected by the decrease in reflected power from the cavity. The power incident on the sample was about 10 mw. The resonance linewidth did not change when the incident power was reduced to 1 mw, indicating that saturation effects were absent. Reflected power vs H_{DC} was plotted for the field range 0 to 10 koe for a large number of crystal orientations, but with H_{DC} restricted to the (110) plane. It was found that some of the observed resonances were very sensitive functions of angle; in order to keep track of their behavior, the angle increment had to be about five degrees.

D. EXPERIMENTAL RESULTS

The DC magnetic field required to excite resonance has been plotted as a function of field direction for the five X-band frequencies. The results are shown in Fig. 15(a-e). It is evident that in all cases, more than one resonance was observed. For the two lowest frequencies, there are many resonances. Most of the resonances can be tracked over a wide range of angle. By comparing the shapes of the curves, it is possible to correlate some of the resonances as a function of frequency. In this manner, it has been possible to construct plots of resonant frequency vs H_{DC} for two of the symmetry axes of the crystal – the [111] and [100] axes. The data for the [111] axis have been superimposed on the theoretical curves of Fig. 13 for comparison. It is interesting to note that there are no experimental points corresponding to the case of M parallel to H. Secondly, the experimental points are in reasonable agreement with the resonance theory, but correspond to the spins lying near to the other [111] axis in the (110) plane. The theoretical curve for the field dependent mode reported by Freiser, et al.,[2] has also been appended. It does not appear possible to excite this mode below about 12 Gcps for the [111] axis.

The graph of resonant frequency vs H_{DC} for H_{DC} parallel to the [100] axis is shown in Fig. 16. Many more resonances were observed for this case than for the [111] case. Again, five of the

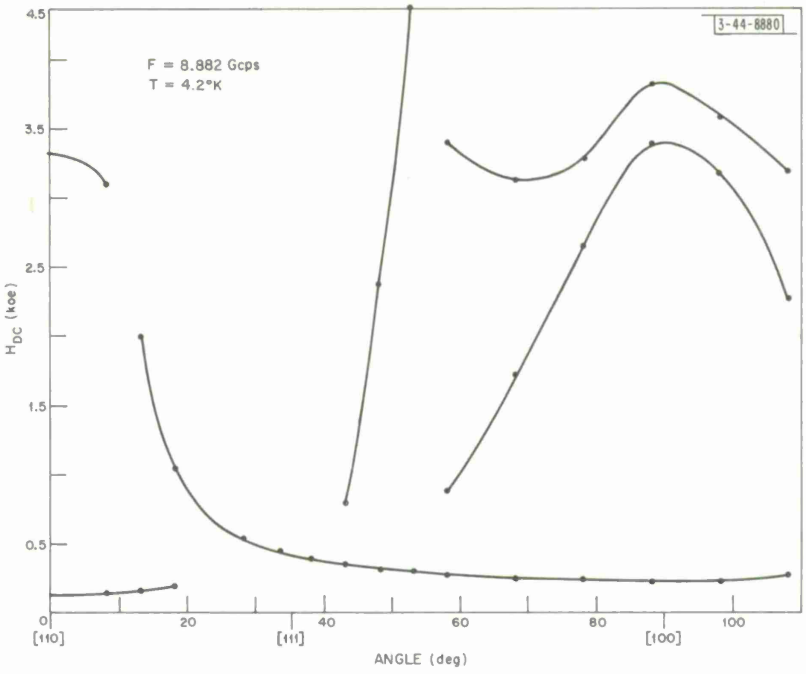

(a)

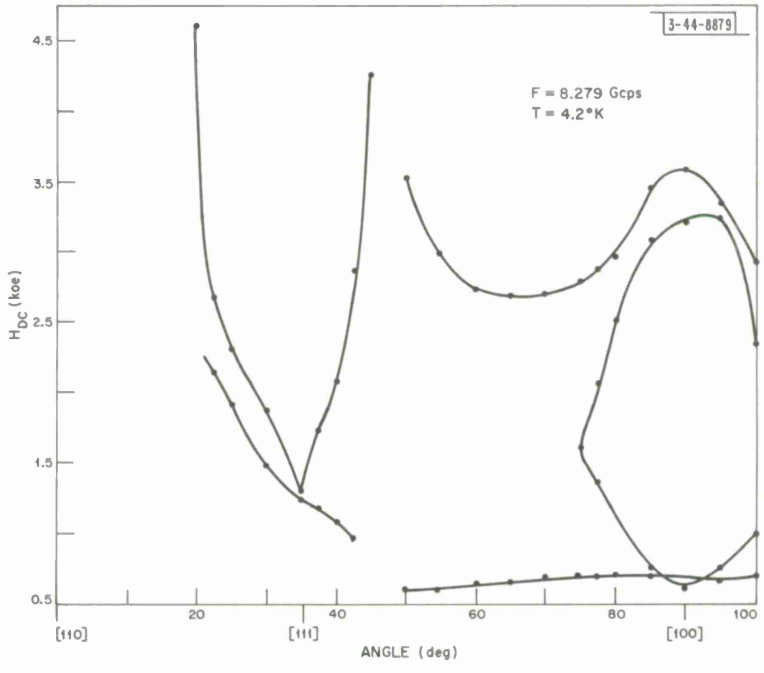

(b)

Fig. 15(a-e). DC magnetic field required for resonance vs angle.

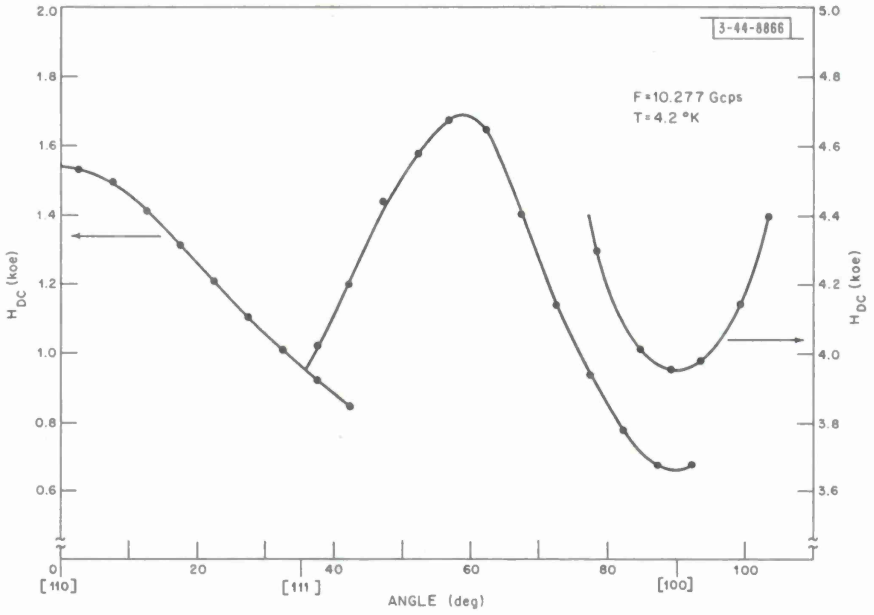

(c)

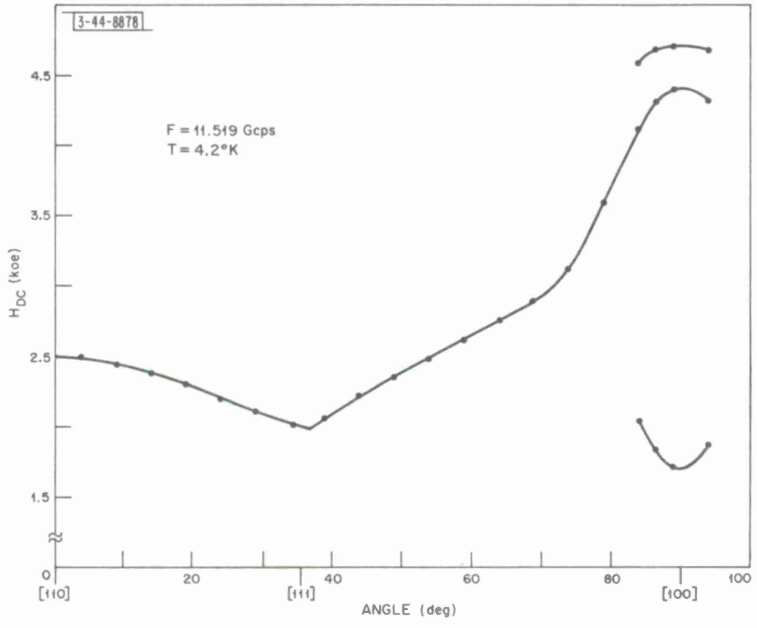

(d)

Fig. 15. Continued

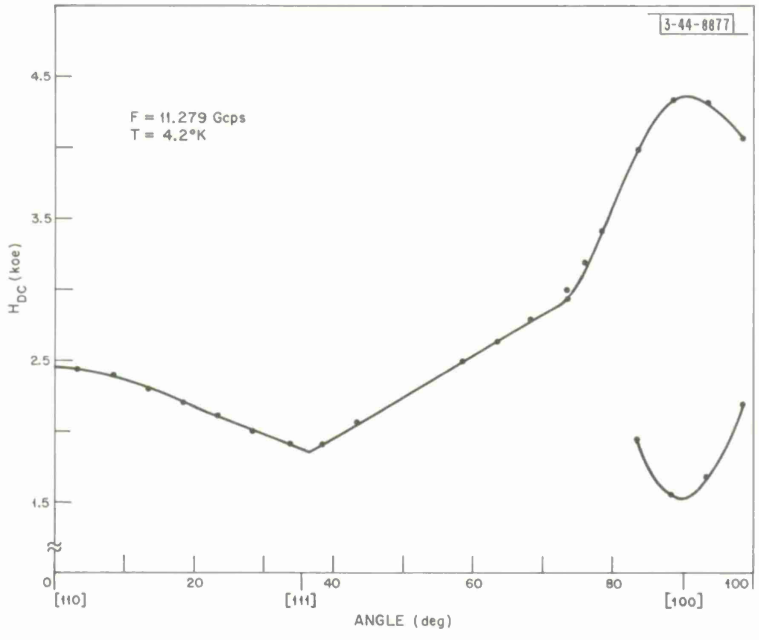

(e)

Fig. 15. Continued.

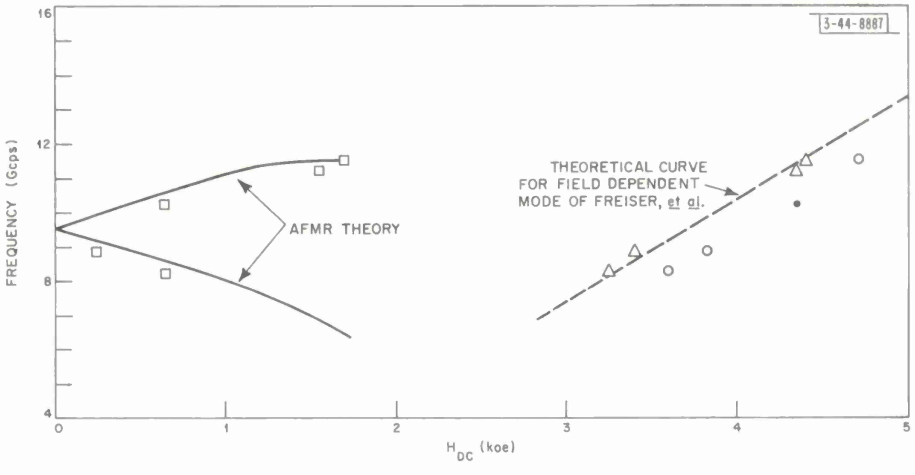

Fig. 16. Observed resonances for H_{DC} parallel to [100] axis.

resonances seem to agree fairly well with the resonance theory. In this case, the theory predicts only one pair of mode branches. By studying the curves in Fig. 15(a-e), it has been possible to group most of the remaining points into two families which seem to belong to different modes of resonance. One group falls very close to the theoretical plot of Freiser's field dependent mode. The second group seems to fall on a line parallel to the first group.

The intercept of the curve of AFMR frequency vs H_{DC} on the frequency axis is nearly equal to $\gamma\mu_o[2H_{ex}(H_N + H_a)]^{1/2}$. Hence, extrapolation of the experimental data provides an estimate of this quantity. Unfortunately, there are only five data points, but an extrapolation indicates that the intercept is at 9.3 Gcps. This is to be compared with a frequency of 9.65 Gcps which was calculated by using the data of Freiser, et al.[2] The discrepancy can be accounted for by a 7-percent difference in the value of H_{ex} (or a difference in H_a). Note that this is consistent with a similar discrepancy noted in the susceptibility data.

The shape of the plots of resonance field vs direction of applied field gave an excellent check on the accuracy of the orientation of the crystal, since the curves should have mirror symmetry about the zero and 90° points. The curves in Fig. 15(a-e) have been replotted with the angular corrections, which did not exceed 3° in any of the experiments.

CHAPTER V
EXCITATION OF SPIN WAVES BY PARALLEL PUMPING

A. MEASUREMENT OF SPIN WAVE LINEWIDTH BY PARALLEL PUMPING

Spin wave instability and premature saturation of the AFMR have been analyzed by Heeger and Pincus.[7] According to their theory, the instability threshold is given by

$$h_{crit} = 4\Delta H_o\left(\frac{\gamma\mu_o\Delta H_k}{\omega_o}\right)^{1/2}$$

where ΔH_o is the uniform mode linewidth, ΔH_k is the spin wave linewidth, and ω_o is the AFMR frequency.

Saturation of AFMR in $KMnF_3$ has been observed by Heeger[9] who found that the onset of saturation occurred at a very low threshold – on the order of 1 mw. He inferred that the spin wave linewidth was on the order of 5×10^{-3} oe, compared with 40 oe for the uniform mode. Naiman and Lawrence[16] have observed a very long relaxation time for spin flopping in the antiferromagnet $CuCl_2 \cdot H_2O$ and have compared their results to Heeger's. The question arises whether similar saturation effects occur for $RbMnF_3$. Thus, it was proposed that the spin wave linewidth for $RbMnF_3$ be estimated by measuring the threshold RF magnetic field for longitudinally pumped spin waves.

Morgenthaler[17] and Schlömann[18] first proposed that spin waves at half the pumping frequency could be parametrically excited by the application of an RF driving field parallel to the DC magnetizing field. Morgenthaler[19] has extended his analysis to include two-sublattice systems and, in particular, has derived an expression for the instability threshold.[20,21]

First order nonlinear coupling processes are assumed to exist so that

$$\omega_p = |\omega_1| + |\omega_2| \quad \text{and} \quad \vec{k}_1 = -\vec{k}_2 \quad .$$

The terms ω_1 and ω_2 are the two magnon frequencies, $\vec{k}_1$ and $\vec{k}_2$ are the respective wave vectors, and ω_p and $\vec{k}_p$ are the corresponding pump parameters. (Higher order processes can exist, but these generally have higher thresholds than first order processes.) Thus, the net magnetization of each lattice may be represented by a steady state component plus a small component due to a standing spin wave. The equation of motion has additional terms compared to the uniform precession case ($k_i = 0$) which arise because of the nonzero divergence of $\vec{M}$. Also included is a term due to the RF driving field, and a damping term of the Landau-Lifshitz form. The analysis, based on a perturbation technique, shows that the pump acts to overcome the loss in the system. To a first approximation, it does not shift the normal mode frequencies, which are found by setting the pump amplitude and loss equal to zero in the equation of motion.

Determination of the critical field for the onset of instability involves finding a solution to the equation of motion for which the pump provides just sufficient power to overcome the loss terms. The two possible frequency relationships, corresponding to degenerate and nondegenerate magnon instabilities, are

$$\omega_1 = \omega_2 = \omega_{ki} \quad \text{and} \quad \omega_i = \omega_{ki} \quad .$$

Since the nondegenerate case can be expected to have a higher threshold, we shall consider only degenerate magnon instabilities. For the antiferromagnet, it is found that

$$h_{crit} = \frac{4\Delta H_k \omega_k}{\omega_M \sin^2\psi} \sqrt{\frac{\omega_a + 2\omega_{ex} + (\lambda_{11} + \lambda_{12})\, k^2 \omega_M + \omega_M \sin^2\psi}{\omega_a + (\lambda_{11} - \lambda_{12})\, k^2 \omega_M}} \tag{15}$$

and the normal mode frequencies are

$$\omega_k = \{[\omega_a + (\lambda_{11} - \lambda_{12})\, k^2 \omega_M]\, [\omega_a + 2\omega_{ex} + (\lambda_{11} + \lambda_{12})\, k^2 \omega_M + \omega_M \sin^2\psi]\}^{1/2} \pm \omega_H \tag{16}$$

$$\cong \sqrt{2\omega_{ex}[\omega_a + (\lambda_{11} - \lambda_{12})\, k^2 \omega_M]} \pm \omega_H \tag{17}$$

where $2\Delta H_k$ is the spin wave linewidth,

$$\omega_k = \frac{\omega}{2}\, p$$

$$\omega_{ex} = \gamma \mu_o W_{12} M$$

$$\omega_H = -\gamma \mu_o H_{DCz}$$

$$\omega_M = -\gamma \mu_o M$$

$$\omega_a = -\gamma \mu_o H_a$$

ψ is the angle between the propagation vector $\vec{k}$ and the z-axis, and λ_{11}, λ_{12} are the coefficients of the next higher order terms in the molecular field expansion. The analysis assumes that the steady state component of the magnetization is parallel to the easy axis and that the parallel susceptibility is zero. Since ω_k appears in the numerator of Eq. (15), it is evident that the mode with the lower frequency has the lower threshold. For the lower frequency, the threshold may be expressed as the difference of two quantities:

$$h_{crit} = \frac{4\Delta H_k}{\omega_M \sin^2\psi}\, [\omega_a + 2\omega_{ex} + (\lambda_{11} + \lambda_{12})\, k^2 \omega_M + \omega_M \sin^2\psi]^{1/2} \times \left[\sqrt{2\omega_{ex}} - \frac{\omega_H}{\sqrt{\omega_a + (\lambda_{11} - \lambda_{12})\, k^2 \omega_M}}\right] . \tag{18}$$

The first quantity increases with k. The second quantity decreases with k, since its denominator is a more sensitive function of k than the numerator. Hence, it follows that the magnons for which $k \cong 0$ have the lowest threshold. Further, Eq. (18) predicts that for $k \cong 0$ magnons, h_{crit} is zero when $H_{DC} = \sqrt{2H_a H_{ex}}$, which is the condition for spin flopping derived in Ch. III. However, by using the more exact expression for ω_k given by Eq. (16), it is found that h_{crit} approaches a finite limit equal to $2\Delta H_k$ as H_{DC} approaches (but is less than) $\sqrt{2H_a H_{ex}}$.

In summary, the threshold field is lowest for $k \cong 0$ magnons propagating in the x-y plane ($\psi = 90°$). It can be reduced to a small value by adjusting the DC magnetic field to be almost equal to, but less than, the flopping field. Because of the dependence of ω_k on H_{DC}, this implies that the frequency of the pump is constrained to be correspondingly low. Measurement of the threshold field provides a direct method of determining ΔH_k, which enters into the threshold equation, provided that the other parameters are known.

In order to predict the required RF power and frequency for such an experiment with $RbMnF_3$, the values H_a and H_{ex} were taken from Ref. 2. The exchange constants W_{11} and W_{12} were

calculated from the data to be −95 and −233, respectively. The exchange constants λ_{11} and λ_{12} were obtained, starting from the expression for the exchange energy:

$$\mathcal{H}_{ex} = -2J_{ij}\vec{S}_i \cdot \vec{S}_j$$

where J_{ij} is the exchange integral. By expanding $\vec{S}_i$ and $\vec{S}_j$ into Taylor series and assuming that only nearest-neighbor interactions are important, it may be shown that

$$\lambda_{11} = \frac{W_{11}L^2}{3} \quad , \quad \lambda_{12} = \frac{W_{12}L^2}{6}$$

where L is the lattice constant.

The spin wave manifold has been plotted in Fig. 17 for a fixed value of H_{DC}. The shape is similar to the spin wave manifold for a ferrimagnetic material, although the curves are nearly degenerate for small values of k. Also, an increase in H_{DC} shifts the curves parallel to the ω_k axis toward the origin rather than away from the origin as in the ferrimagnetic case. This is illustrated in Fig. 18, where a family of dispersion curves for different values of H_{DC} has been plotted. Only the curves for $\sin\psi = 1$ are shown; ΔH_k was assumed to be 1 oe.

The propagation factor was computed for various values of ω_k, for a given applied DC field, by using Eq. (17). Corresponding values of h_{crit} were then calculated by using Eq. (15) and are plotted in Fig. 19. It is seen that h_{crit} increases very rapidly with frequency and the applied power, which is proportional to $(h_{crit})^2$, becomes prohibitively large. Two curves are shown corresponding to two values of ΔH_k (1 and 0.01 oe). Only the curves for $\sin\psi = 1$ have been plotted since these have the lowest threshold. The value of H_{DC} was chosen to be within 5 oe of spin flop in order to limit h_{crit} to reasonably attainable values in the VHF region of the spectrum. This choice could be unreasonable on two counts: (1) the requirement of extreme

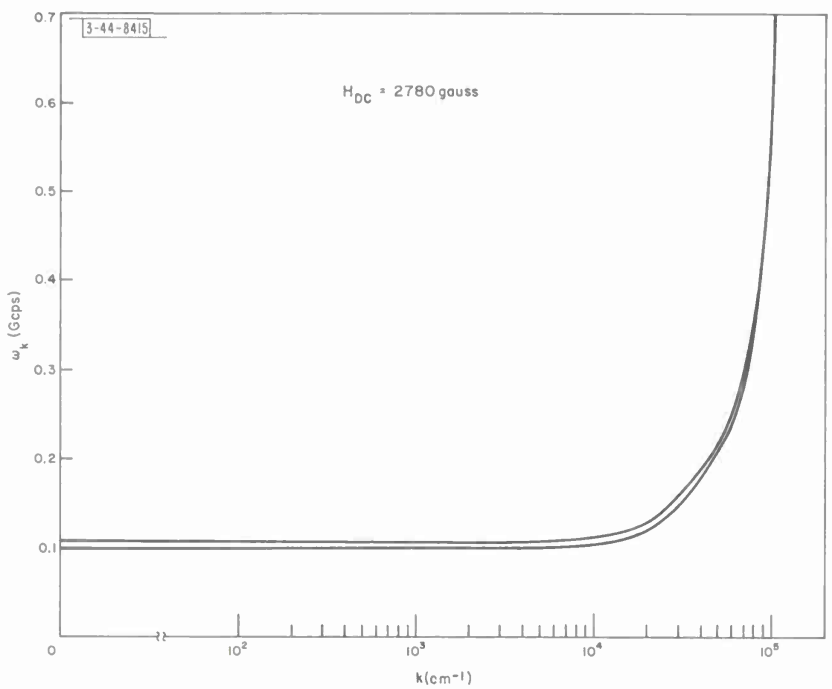

Fig. 17. Spin wave frequency vs spin wave number.

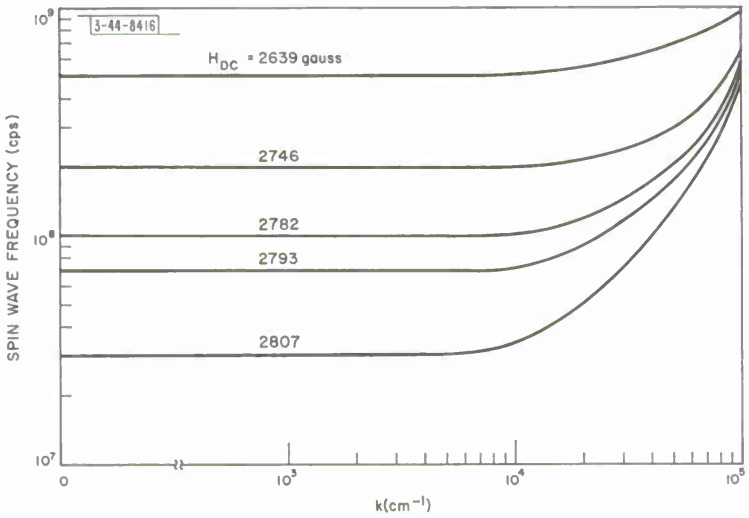

Fig. 18. Spin wave frequency vs k.

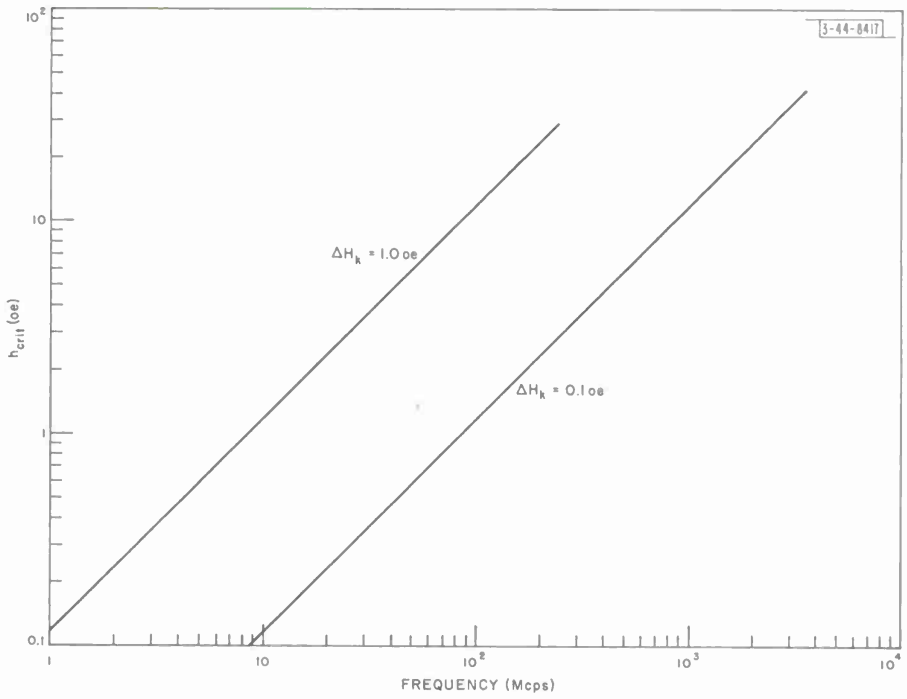

Fig. 19. h_{crit} vs pump frequency.

stability in the applied DC field, (2) dislocations in the crystal could cause H_a and H_{ex} to be nonuniform, resulting in an ill-defined value of flopping field.

The choice of the operating temperature at which to perform parallel pumping experiments is quite important because the spin wave linewidth exchange and anisotropy fields all vary with temperature and affect h_{crit} correspondingly. The most important variable is the anisotropy which, according to Ref. 2, is one-hundredth of its 0°K value at 77°K. Hence, considering only the variation of H_a, h_{crit} at liquid nitrogen temperature will be ten times its value at liquid helium temperature.

B. MEASUREMENT TECHNIQUE

From the foregoing analysis, it was concluded that by setting the DC field to within a few oersteds of the flopping field, the instability threshold would be attained at VHF frequencies with modest power levels if ΔH_k were on the order of 0.1 oe. Accordingly, a parallel pumping experiment was designed to operate at a frequency of 30 Mcps. This experiment was a lumped circuit version of the usual microwave parallel pumping experiment, its principle of operation being the detection of a sudden increase in χ'' when the instability threshold is exceeded. The sample was placed on the axis of a solenoid which was part of an RF bridge circuit. An increase in the loss of the sample would then cause an unbalance of the bridge. This type of measurement is similar to the measurement of NMR.[22-24] Two NMR bridge circuits were considered. The first, used by Bloembergen, et al.,[22] utilizes a circuit in which the responses of two identical shunt-tuned coils, one containing the sample, are balanced against each other. The phases and amplitudes of each half of the bridge are adjusted for a null at the summing point. The three disadvantages of the scheme are: (1) to avoid excessive drift, the reference channel should have the same environment as the sample channel, (2) one of the channels must contain a $\lambda/2$ cable to invert the phase, or a transformer must be used, (3) since the amplitude and phase adjustments are not independent, the adjustment procedure is very tedious.

In the experiment, the detection scheme used the bridged-T circuit[25] illustrated in Fig. 20. The sample coil L is situated in one arm of the bridge which is nonresonant. The bridge is balanced by two independent adjustments: The phase balance is obtained by varying the capacitor C; the amplitude balance is determined by the variable capacitor C'. The conditions for balance are independent of the source and load impedances.

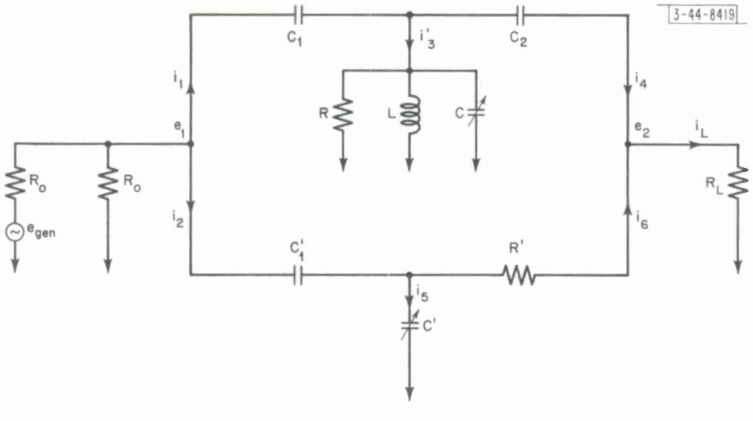

Fig. 20. Bridged-T circuit.

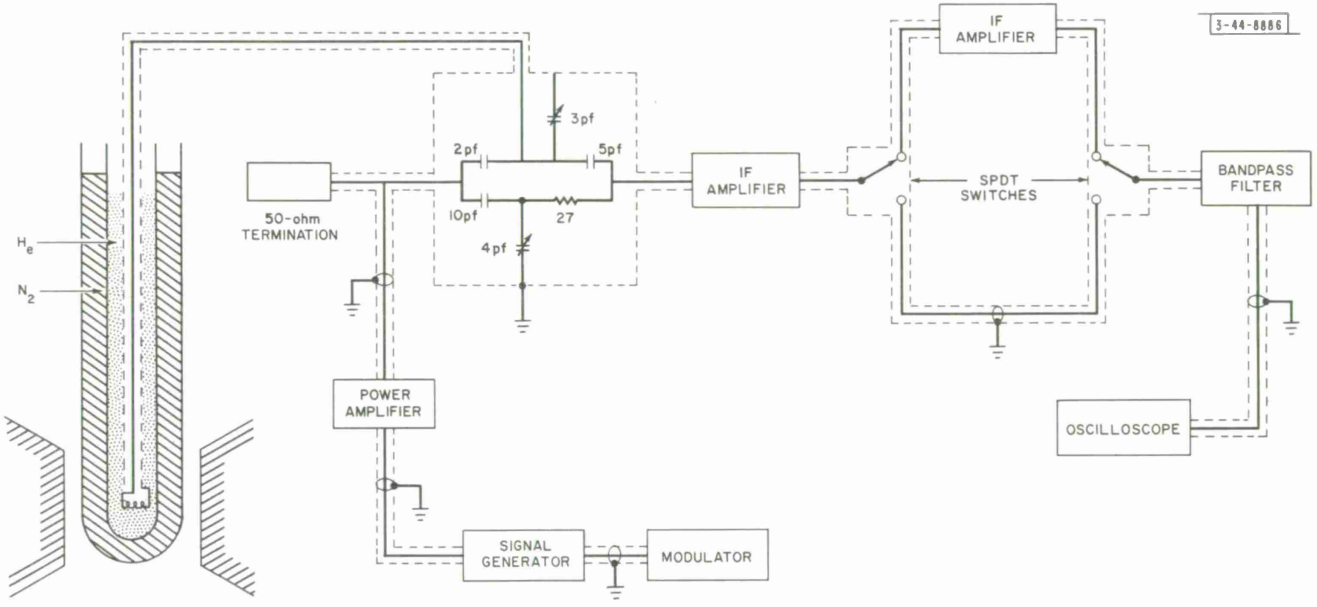

Fig. 21. Block diagram of parallel pumping experiment.

Although the bridged-T circuit is inherently a narrow band device, this was not important, apart from stability considerations, since the experiment was performed at a single frequency. The practical limit of sensitivity achievable, which is a function of the depth of the null, is limited to about −60 db because of the difficulty of maintaining the balance.

The conditions for balance are

$$\frac{1}{R} = \omega^2 C_1 C_2 \left[1 + \frac{C'}{C'_1}\right] R' \tag{19}$$

and

$$\frac{1}{\omega^2 LC} = 1 + \frac{C_1}{C} + \frac{C_2}{C}\left(1 + \frac{C_1}{C'_1}\right) \tag{20}$$

where R is the equivalent shunt loss of the coil, and C is the shunt-tuning capacitor. The Q of the inductor is given by

$$Q = \frac{R}{\omega L} = \frac{C + C_1 + C_2\left(1 + \frac{C_1}{C'_1}\right)}{\omega C_1 C_2 \left(1 + \frac{C'}{C'_1}\right) R'} \quad .$$

A block diagram of the parallel pumping experiment is shown in Fig. 21. The sample coil was immersed in liquid helium and located between the pole pieces of a 6-inch Varian electromagnet. Several different coil designs were used in an effort to improve the filling factor, but each had an inductance of about 1 μh and required about 20 to 25 pf of shunt capacitance for balancing purposes.

The bridged-T circuit was located immediately above the dewar vessel in order to minimize the length of the connection to the coil. A special low capacitance coaxial transmission line was used for the connection. The center conductor was a fine wire supported by polystyrene foam; the outer conductor was stainless steel, copper plated on the inside to a thickness of a skin depth. When cooled, the Q of the coaxial line plus coil was 320. The signal, which could be square wave or pulse modulated, was obtained from a stable generator at the milliwatt level and was amplified to a level of about 12 watts by a class C tuned power amplifier. The out-of-balance signal from the bridge circuit was amplified by two IF strips each having 30 db of gain. The output was displayed directly on an oscilloscope.

Because of the sensitivity of the equipment, an increase in loss of the sample, equivalent to a sample Q of about 1500, could be detected. The sensitivity to reactive changes was about one part in 2500 (0.01 pf change in C'). This corresponded to a μ'' of 0.01 or a μ' of 5×10^{-3} for 0.25 gram of $RbMnF_3$ with the coil wound on the sample.

The orientation of the sample was chosen so that a [111] axis was parallel to the axis of the solenoid which was also parallel to H_{DC}.

C. EXPERIMENTAL RESULTS

With the coil and sample cooled to 4.2°K and the signal power set for maximum output, the DC magnetic field was increased exceedingly slowly over the range 0 to 10 koe. A slight reactive unbalance was observed which was attributed partly to the increase of χ' with H_{DC} and partly to a spurious effect which was observed even in the absence of the sample. There was no unbalance

which could be attributed to an increase in χ''. The DC field range 2 to 3 koe, which embraces the spin flop value, was examined very carefully, but there was no apparent instability effect.

It was estimated that the maximum intensity of the RF magnetic field in the coil was 0.75 oe, which should have been sufficient to exceed the instability threshold provided that ΔH_k was not greater than 0.375 oe.

Recognizing the probable difficulty of lining up the magnetization with the applied DC field, as concluded from the DC susceptibility measurements, the negative experimental result was not taken to imply that the spin wave linewidth was much larger than expected, but that the basic requirements for parallel pumping were not satisfied.

The direction of H_{DC} with respect to the coil axis was changed, with the hope that this would cause M to line up parallel to the RF field, and the experiment was repeated. However, no combination of magnitude or angle of applied field, or magnitude of RF field, resulted in the observation of spin wave instabilities.

CHAPTER VI
CONCLUSIONS

Magnetic susceptibility measurements on $RbMnF_3$ samples yielded a value for the exchange field H_{ex} in good agreement with, but about 7 percent less than, previously published data. The measured value for the Néel temperature, 94°K, was significantly higher. The susceptibility, as a function of applied DC field, showed no abrupt discontinuity, although an analysis of the static equilibrium position of the magnetization indicates that this is possible under certain conditions.

Antiferromagnetic resonance theory, together with the static equilibrium analysis for the restricted case of H_{DC} lying in a (110) plane, has permitted prediction of the AFMR spectrum. The theory is in fair agreement with the experimental data for the [111] and [100] directions. Observed resonances for the case of H_{DC} parallel to the [111] axis are consistent with the interpretation that there were few, if any, spins parallel to H_{DC}. The negative result of an experiment designed to excite spin wave instabilities by the parallel pumping technique is consistent with this interpretation.

The value of the quantity $\sqrt{2H_{ex}(H_a + H_N)}$, obtained by extrapolating the experimental AFMR data to zero DC field, is about 3.5 percent lower than the value calculated from published data. This discrepancy is consistent with that found in the susceptibility measurements.

APPENDIX
DERIVATION OF THE TRANSFORMATION MATRIX [T]

Let (O, X, Y, Z) be the coordinate system referred to the cube edges, and let the (X, Y, Z) axes be rotated through an angle θ about a line passing through the origin and perpendicular to the (110) plane of interest, i.e., about a [110] axis (see Fig. A-1). Also, let (o, x, y, z) be the new coordinate system, and let $\hat{X}, \hat{Y}, \hat{Z}$ and $\hat{x}, \hat{y}, \hat{z}$ be unit vectors along the respective axes. Further, let $\hat{V}$ be a unit vector along the [110] direction in the (O, X, Y, Z) system with $\hat{m}$ the corresponding unit vector in the (o, x, y, z) system, and let $\hat{U}$ be a unit vector perpendicular to the (110) plane at the origin in the (O, X, Y, Z) system with $\hat{\ell}$ the corresponding unit vector in the (o, x, y, z) system.

Then

$$\hat{V} = \frac{\hat{Y} + \hat{X}}{\sqrt{2}} \qquad \hat{U} = \frac{\hat{Y} - \hat{X}}{\sqrt{2}}$$

$$\hat{m} = \frac{\hat{y} + \hat{x}}{\sqrt{2}} \qquad \hat{\ell} = \frac{\hat{y} - \hat{x}}{\sqrt{2}}$$

where

$$\hat{U} = \hat{\ell}$$

$$\hat{V} = \hat{z} \sin\theta + \hat{m} \cos\theta$$

$$\hat{Z} = \hat{z} \cos\theta - \hat{m} \sin\theta \quad .$$

It follows that

$$\hat{Y} - \hat{X} = \hat{y} - \hat{x}$$

$$\frac{\hat{Y} + \hat{X}}{\sqrt{2}} = \hat{z} \sin\theta + \frac{(\hat{x} + \hat{y})}{\sqrt{2}} \cos\theta$$

$$\hat{Z} = \hat{z} \cos\theta - \frac{(\hat{y} + \hat{x})}{\sqrt{2}} \sin\theta \quad .$$

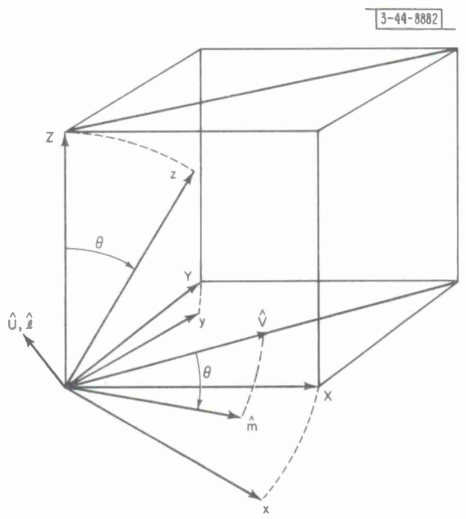

Fig. A-1. Illustration of coordinate rotation.

By rearranging the last three equations and writing them in matrix form,

$$\begin{bmatrix} \hat{X} \\ \hat{Y} \\ \hat{Z} \end{bmatrix} = \begin{bmatrix} \left(\frac{\cos\theta + 1}{2}\right) & \left(\frac{\cos\theta - 1}{2}\right) & \frac{\sin\theta}{\sqrt{2}} \\ \left(\frac{\cos\theta - 1}{2}\right) & \left(\frac{\cos\theta + 1}{2}\right) & \frac{\sin\theta}{\sqrt{2}} \\ \frac{-\sin\theta}{\sqrt{2}} & \frac{-\sin\theta}{\sqrt{2}} & \cos\theta \end{bmatrix} \begin{bmatrix} \hat{x} \\ \hat{y} \\ \hat{z} \end{bmatrix}$$

or

$$[\hat{X}] = [T]\,[\hat{x}] \quad .$$

Hence,

$$[\hat{x}] = [T]^{-1}\,[\hat{X}]$$

where

$$[T]^{-1} = \begin{bmatrix} \left(\frac{\cos\theta + 1}{2}\right) & \left(\frac{\cos\theta - 1}{2}\right) & \frac{-\sin\theta}{\sqrt{2}} \\ \left(\frac{\cos\theta - 1}{2}\right) & \left(\frac{\cos\theta + 1}{2}\right) & \frac{-\sin\theta}{\sqrt{2}} \\ \frac{\sin\theta}{\sqrt{2}} & \frac{\sin\theta}{\sqrt{2}} & \cos\theta \end{bmatrix} \quad .$$

ACKNOWLEDGMENT

The author wishes to express his appreciation to Professor F. R. Morgenthaler for his continued guidance. The resonance experiments were performed in conjunction with Dr. P. H. Cole who also provided valuable suggestions concerning the theoretical analysis.

Special acknowledgment is due to Dr. M. Kestigian of the Sperry Rand Research Center who generously provided the crystals of $RbMnF_3$, without which this research would not have been possible.

The author would also like to thank R. Santoro for his helpful comments on the use of the vibrating sample magnetometer, R. Mills for providing the x-ray service and cutting the $RbMnF_3$ crystals, Professor R. E. Newnham for discussions concerning the x-ray analysis, and the various members of the Microwave and Quantum Magnetics Group of the Center for Materials Science and Engineering for their beneficial discussions.

The author is deeply indebted to J. DiBartolo, Jr., who contributed important items of hardware used in the parallel pumping experiment, to C. P. Hartwig who generously lent much of the X-band equipment used in the resonance experiments, and to T. Stewart and P. Kelleher who provided valuable support effort.

REFERENCES

1. D.T. Teaney and M.J. Freiser, "Discovery of a Simple Cubic Antiferromagnet; Antiferromagnetic Resonance in $RbMnF_3$," Phys. Rev. Letters 9, 212 (1962).
2. M.J. Freiser, et. al., "Magnetic Resonance Studies of the Cubic Antiferromagnet, $RbMnF_3$," Proceedings of the International Conference on Magnetism, Nottingham, England, 1964 (The Institute of Physics and the Physical Society, London).
3. L. Néel, Proceedings of the International Conference on Theoretical Physics, University of Kyoto, 1953 (Maruzen, Tokyo).
4. T.R. McGuire, "Magnetic Susceptibility of $RbMnF_3$," Meeting of the American Physical Society, New York, January 1963.
5. T. Nagamiya, K. Yosida and R. Kubo, "Antiferromagnetism," Advances in Physics 4, 1 (January 1955).
6. F. Keffer and C. Kittel, "Theory of Antiferromagnetic Resonance," Phys. Rev. 85, 2 (1952).
7. A.J. Heeger and P. Pincus, "Spin Wave Instability and Premature Saturation in Antiferromagnetic Resonance," Phys. Rev. Letters 10, 2 (1963).
8. H. Suhl, "The Non Linear Behavior of Ferrites at High Microwave Signals," Proc. IRE 44, 10 (1956).
9. A.J. Heeger, "Spin Wave Instability and Premature Saturation in Antiferromagnetic Resonance," Phys. Rev. 131, 608 (1963).
10. L.F. Bates, Modern Magnetism (Cambridge University Press, New York, 1951), p. 151.
11. R. Hunt, "Magnetic Anneal Effects in Some Garnets," Ph.D. Thesis, Department of Electrical Engineering, M.I.T. (1964).
12. R. Santoro, "Magnetic Properties of the Olivines," Ph.D. Thesis, Department of Electrical Engineering, M.I.T. (1965).
13. S. Foner, "Vibrating Sample Magnetometer," Rev. Sci. Instr. 30, 548 (1959).
14. J.H. Van Vleck, "On the Theory of Antiferromagnetism," J. Chem. Phys. 9, 85 (1941).
15. F.R. Morgenthaler, "Stability of the Néel Ground State in a Two-Sublattice Ferrimagnet," Phys. Rev. Letters 12, 475 (1964).
16. C.S. Naiman and T.R. Lawrence, "Spin-Flopping Relaxation Time in $CuCl_2 \cdot 2H_2O$," J. Appl. Phys. 36, 3 (1965).
17. F.R. Morgenthaler, "Survey of Ferromagnetic Resonance in Small Ferromagnetic Ellipsoids," J. Appl. Phys. 31, 955 (1960).
18. E. Schlömann, J.J. Green and U. Milano, "Recent Developments in Ferromagnetic Resonance at High Power Levels," J. Appl. Phys. 31, 3865 (1960).
19. F.R. Morgenthaler, "Longitudinal Parametric Excitation of Magnons in a Two-Sublattice Ferromagnetic Crystal," Phys. Rev. Letters 11, 239(E), 69 (1963).
20. Laboratory for Insulation Research, M.I.T., Progress Report No. 33 (July 1963), p. 79.
21. F.R. Morgenthaler, to be published in J. Appl. Phys.
22. N. Bloembergen, E.M. Purcell and E.M. Pound, "Nuclear Magnetic Resonance Absorption," Phys. Rev. 73, 679 (1948).
23. H. L. Anderson, "Precise Measurement of the Gyromagnetic Ratio of He^3," Phys. Rev. 76, 1460 (1949).
24. G.E. Pake, "Fundamentals of Nuclear Magnetic Resonance Absorption," Am. J. Phys. 18, 473 (1950).
25. W.N. Tuttle, "Bridged-T and Parallel-T Null Circuits for Measurements of Radio Frequencies," Proc. IRE 28, 23 (1940).

DOCUMENT CONTROL DATA – R&D

(Security classification of title, body of abstract and indexing annotation must be entered when the overall report is classified)

1. ORIGINATING ACTIVITY *(Corporate author)* Lincoln Laboratory, M. I. T.	2a. REPORT SECURITY CLASSIFICATION Unclassified 2b. GROUP None

3. REPORT TITLE

Magnetic Studies of the Antiferromagnet $RbMnF_3$

4. DESCRIPTIVE NOTES *(Type of report and inclusive dates)*

Technical Report

5. AUTHOR(S) *(Last name, first name, initial)*

Ince, William J.

6. REPORT DATE	7a. TOTAL NO. OF PAGES	7b. NO. OF REFS
14 October 1965	52	25

8a. CONTRACT OR GRANT NO. AF 19(628)-5167 b. PROJECT NO. ARPA Order 498 c. d.	9a. ORIGINATOR'S REPORT NUMBER(S) Technical Report 384 9b. OTHER REPORT NO(S) *(Any other numbers that may be assigned this report)* ESD-TDR-65-493

10. AVAILABILITY/LIMITATION NOTICES

Distribution of this document is unlimited.

11. SUPPLEMENTARY NOTES	12. SPONSORING MILITARY ACTIVITY
None	Advanced Research Projects Agency, Department of Defense

13. ABSTRACT

Magnetic properties of the antiferromagnet $RbMnF_3$ have been studied. Below T_N, the magnetic ions order into a two-sublattice system with the spins antiparallel. $RbMnF_3$ exhibits high exchange and low anisotropy; the form of the anisotropy surface is cubic. Consequently, for applied DC magnetic fields less than about 3000 oe, the static equilibrium position of the sublattice magnetization is, in general, multivalued.

Measurements of the DC susceptibility χ have been made on powder and single crystal specimens of $RbMnF_3$ for the range of applied field 0 to 12 koe and over the temperature range 4.2 to 300°K. The observed value of T_N was about ten degrees higher than the previously published value. When plotted as a function of applied field, $\chi_{[111]}$ shows no abrupt discontinuity analogous to the spin flopping exhibited by uniaxial antiferromagnets.

A simple model, in which H_{DC} and M are restricted to the (100) plane, has enabled solutions of the static equilibrium problem to be obtained. X-band resonance experiments are reported, and a resonance theory is presented which incorporates the equilibrium solutions. The predicted antiferromagnetic resonance spectrum shows reasonable agreement with the experimental data. The possibility of parallel pumping spin waves in $RbMnF_3$ is considered, and an attempt to measure the spin wave linewidth is described.

14. KEY WORDS

antiferromagnetic materials magnetic properties magnetic resonance

Printed by
United States Air Force
L. G. Hanscom Field
Bedford, Massachusetts